POLITECNICO DI TORINO

Master's Degree in Aerospace Engineering

Master's Degree Thesis

INVESTIGATION OF SENSOR FAULTS IN A GAS TURBINE

Supervisors

Prof. Andrea FERRERO

Prof. Christian KOCH

Candidate

Giuseppe SOLARO

Ottobre 2022

Summary

When testing gas turbine engines, a variety of flow parameters must be monitored. The precise measurement of total pressure and total temperature values is critical for evaluating the performance of the entire engine as well as individual engine components. Moreover, these parameters are used to define the control law and the engine health monitoring in an installed engine in operation conditions. The actual sensor design is often challenging due to the high temperatures and flow velocities within a gas turbine. In this study, a detailed literature review is reported, in order to describe the inaccuracy of the two systems, the temperature and the pressure measurement system, given by the contributions of each component in the chain. This review allowed a deeper understanding of the different parameters involved in defining the system's inaccuracy and, moreover, the formulation of inaccuracy forecast highlighted in a modern engine. Regarding the temperature measurement system inaccuracy, a thermocouple in MIMS configuration with an exposed junction was considered. The indicated temperature is primarily influenced by systematic errors caused by the design of the sensor probe, whereas thermocouple drift has a lower impact on the deviation from true temperature: the errors in the individual components of the chain are in the same order as the inaccuracy of the type K thermocouple, therefore, they cannot be neglected. Regarding the pressure measurement system inaccuracy, the probe's design is critical, instead the errors from other components of the pressure chain have little impact, which could be omitted due to the high pressure inside the engine.

Acknowledgements

Desidero ringraziare il Dott.Ing. Christian Koch, mio tutor e guida presso l'ILA (Institut für Luftfahrtantriebe), che con grande disponibilità e competenza ha supportato il mio lavoro grazie ai suoi suggerimenti e le sue preziose indicazioni. Un sentito ringraziamento al Prof. Andrea Ferrero per la fiducia e il sostegno che mi ha dimostrato in questi mesi.

A mio padre,
per essere stato senza saperlo la mia costante forza di volontà.
A mia madre, esempio di forza e caparbietà,
per essere sempre la casa in cui posso tornare e sentirmi al sicuro.
Questo grande traguardo è anche Vostro.

Table of Contents

List of Tables

List of Figures

Acronyms

EGT
Exhaust Gas Temperature

EEC
Electronic Engine Control

FADEC
Full Authority Digital Engine Control

HPC
High Pressure Compressor

HPT
High Pressure Turbine

LPT
Low Pressure Turbine

OGV
Outlet Guide Vane

CCDL
Cross-Channel Data Link

RTDs
Resistance Temperature Devices

TSR
Temperature Sensitive Resistor

emf

electro-motive force

MIMS

Mineral Insulated Metal Sheathed

T_J

total Temperature of the thermocouple Junction

T_T

Free-stream Total Temperature

T_S

Free-stream Static Temperature

R

Recovery factor

Ma_F

Free-stream Mach number

Ma_J

Junction Mach number

Y_v

Velocity error

AE

Area Kiel entry

AB

Area bleed hole

r

overall recovery factor

$\bar{R}$

corrected recovery factor

Y_c

Conduction error

L

Length of thermocouple exposed

D

wire Diameter

Y_r

Radiation error

FS

Full Scale

SIT

Semi-Infinte Tube

DAQ

Data Acquisition system

Introduction

Modern turbine engine control and health management depend on sensing a wide range of quantities throughout the engine, including temperatures, pressures, and vibration, all with varying redundancy, reliability, and accuracy requirements. These values can be used as inputs to control laws as well as to estimate the performance and health of various engine components. The sensors must meet different requirements depending on their function: control sensors require proven extended reliability, accuracy, and speed of response, which makes them extremely expensive for turbine engine applications, while engine health management sensors, on the other hand, do not have the same high-reliability requirements and are frequently not redundant.

This work focuses on technology for temperature and pressure measurements inside the section of the engine; the intent is to provide an overview of the difficulties and issues in obtaining accurate measurements.

The Exhaust Gas Temperature EGT is one of the most important parameters of the turbine section. The severe circumstances in which the turbine runs are most of the difficulties encountered in taking measurements inside the turbine area. This is not surprising given that the turbine is exposed to gases directly from the combustor, which is near the thermodynamic peak temperature and pressure.

Gas turbine trend, which including higher cycle temperatures and pressures, is shown in figure 1.

In addition to the fact that turbine conditions are becoming harsher, there is also a push to reduce uncertainty because uncertainty and transients force the need for margins in the design of turbine engines. Reducing uncertainty is one tactic to increase the level of integration that is practical within a complex propulsion system, as each component or subsystem must be able to function in the worst-case scenario with other components.

The main reasons to monitor continuously the gas turbine signals, pressure and temperature, are:

- cycle performance optimization and power control engine through all the different operational conditions

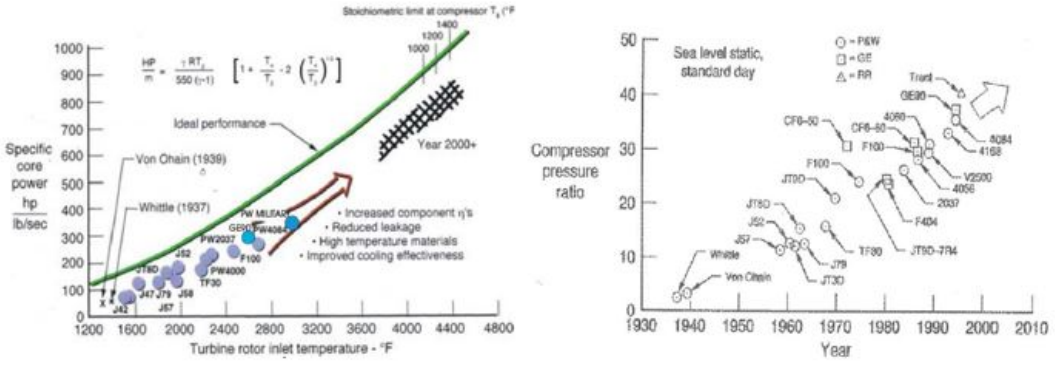

Figure 1: Gas turbine trend, [1]

- health monitoring of high-temperature components limiting over-temperature for increased hot section life. Due to the harsh operating conditions of the turbine, monitoring temperature readings helps to guarantee that material limits aren't exceeded and that the wear can be calculated
- performance evaluation because the knowledge of inlet and exit signals allows to calculate the efficiency of compressors and turbines
- improved engine transient response within thermal cycling limits

Chapter I provides a brief description of the CFM56 and V2500 gas turbine engines, which are chosen like reference engines, along with basic performance data and the engine's leading particulars about sensor instrumentation.

Chapter II presents for the CFM56 engine how the sensor signal from the Electronic Engine Control EEC is handled in terms of utility and fault detection strategy.

Chapter III presents the *temperature measurements system* and the *pressure measurements system* with the related reliability, accuracy, and related problems attached.

Chapter IV presents the test case developed with an evaluation of the forecast results, according to the problems highlighted in the *temperature measurements system* and *pressure measurements system* chapter.

Chapter V summarizes and provides conclusions about the work that has been done. A comparison between values predicted in the test case model developed

and data provided by the literature is presented, identifying existing problems, and proposing further work to settle unsolved discrepancies.

Motivation

The Institute of Aircraft Propulsion Systems operates a remote-controlled model helicopter powered by a gas turbine. In teaching, it is utilized as a test object for engine performance model development based on flight test data. It also serves as a test vehicle for the research of transient condition monitoring. The gas turbine used is a commercial product called PHT-3. The PHT-3 engine on the ground test bed is used as a real-world data generator for the validation of fault and damage detection algorithms. There is currently no logic in place to detect sensor faults or measurement system degradation.

The unknown behavior of malfunctioning sensors and the precise fault variation picked from a list of probable problems are the starting points for this problem.

Objectives

The aim of this thesis is to find out possible sensor faults, how they will affect the sensor signal and how such faults could be simulated on the test bed.

Chapter 1

V2500 and CFM56 Gas Turbine Engine

1.1 V2500 and CFM56 Propulsion Unit

The V2500 and CFM56 are twin-spool, axial flow, high by-pass ratio turbofans series designed primarily for 150 seats, short to medium range aircraft. Both engines incorporate several advanced technology features which include Full Authority Digital Electronic Control - FADEC, with two channels.

The first one was developed in 1983 by five of the world's leading aerospace manufacturers who signed a 30-year collaboration agreement to produce an engine for the single isle aircraft market with the best proven technology that each could provide and it was certified in 1988. Each of the shareholder companies is given the responsibility for developing and delivering one of the five engine modules, as shown in figure 1.1. However, the engines are assembled by the major partners, Rolls Royce and Pratt and Whitney.

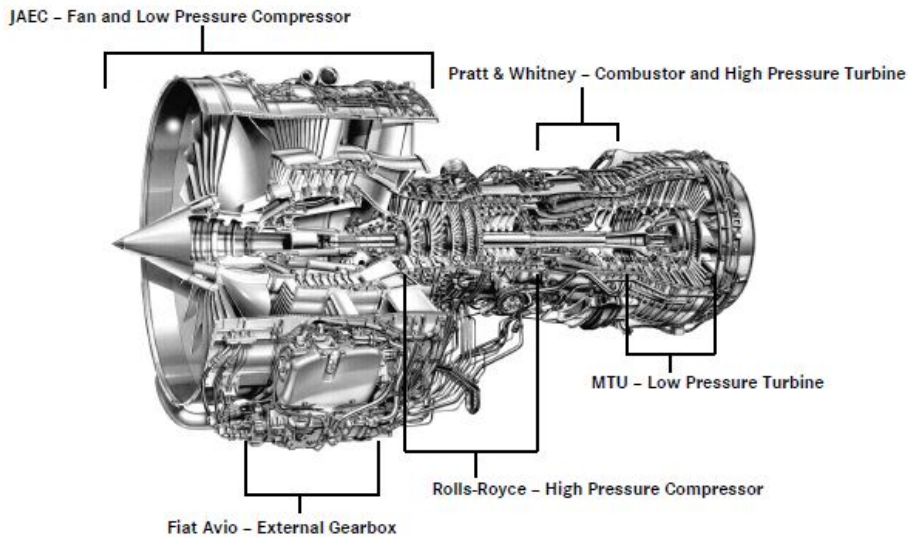

Figure 1.1: IAE V2500 Engine - the responsibility, [2]

The second one is a Franco-American family of high-bypass turbofan aircraft engines manufactured by CFM International. CFMI is a 50-50 joint venture between France's Safran Aircraft Engines (formerly known as Snecma) and the United States' GE Aviation.

Both are in charge of component production, and each has its own final assembly line: GE manufactures the High-Pressure Compressor HPC, combustor, and High-Pressure Turbine HPT, while Safran manufactures the Fan, gearbox, exhaust, and Low-Pressure Turbine LPT. Avio of Italy and Honeywell of the United States manufacture some components.

The propulsion unit - Data is shown below, respectively for the two families of engines: for both engine families, the engine installed on the A320 is taken as a reference.

T.O Thrust	111.205 KN
Total Airflow	355 Kgs/second
By-pass ratio	5.42:1
Overall Pressure ratio	29.4:1
Fan Diameter	160 cm
Engine overall length	320 cm
Engine Weight	2242 Kgs

Table 1.1: Propulsion Unit - Data V2500-A1 Engine, [2] [3]

T.O Thrust	117.877 KN
Total Airflow	397 Kgs/second
By-pass ratio	6:1
Overall Pressure ratio	31.3:1
Fan Diameter	173 cm
Engine overall length	242.31 cm
Engine Weight	2266 Kgs

Table 1.2: Propulsion Unit - Data CFM56-5A3 Engine, [4] [5]

Both engines, used as a comparison to comprehend which are the instrumented stations and the primary technologies implemented in terms of sensors in today's engine, share a number of similar characteristics.

1.1.1 Thermodynamic Stations

The flow in a turbofan engine follows two distinct and independent paths: primary and secondary flows. The primary flow, also known as core flow, enters the engine at the inlet and passes through the Fan near its root, generating a little increase in pressure. The primary air then enters the core via the Booster and HPC, where its pressure is greatly increased (approximately 30 times ambient pressure for both engines), after which it is a mixture with fuel and burned in the combustion chamber, passes through the HPT and LPT, where it expands, and is discharged via the core nozzle.

The secondary flow, also known as by-pass flow, enters the engine at the intake, passes through the Fan on the periphery of its blades, causing a pressure increase, and is then steered by the Outlet Guide Vanes OGVs before being discharged. This flow accounts for roughly 80 % of the total thrust generated in the engine.

The V2500 is a Mixed Exhaust Turbofan while the CFM56 is a Separate Flow Turbofan, which makes a significant difference between the two engines.

- V2500: the core engine 'hot' exhaust and the 'cool' by-pass flow are 'mixed' in the Common Nozzle Assembly before passing through the single propelling nozzle into the atmosphere.

- CFM56: the core engine 'hot' exhaust and the 'cool' by-pass flow pass through a different propelling nozzle into the atmosphere.

An engine map for each one is presented, showing the location of the stations respectively in figure 1.2 for V2500 and in figure 1.3 for CFM56. In table 1.3 are reported for each station the corresponding parts of the engine.

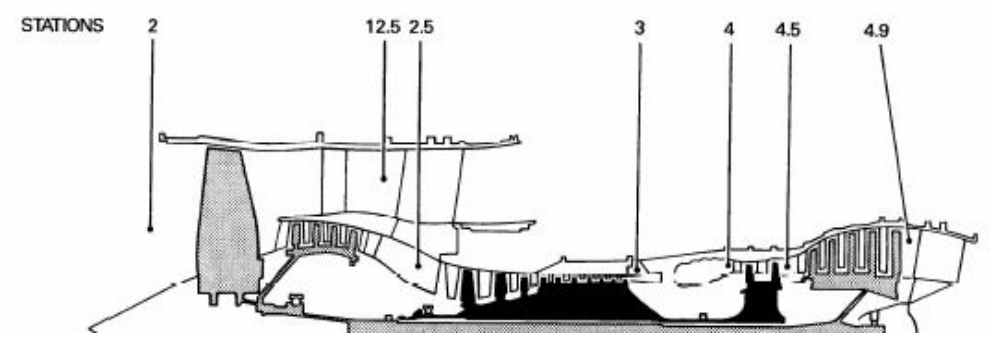

Figure 1.2: V2500-A1 - Thermodynamic stations, [2]

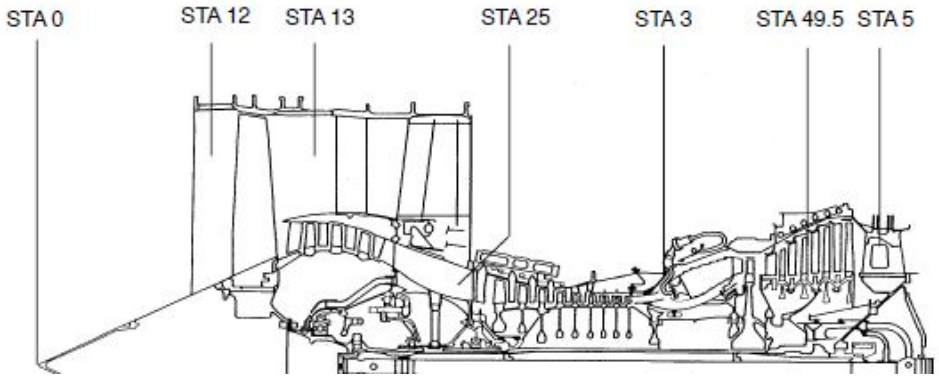

Figure 1.3: CFM56-5A3 - Thermodynamic stations, [4]

-	V2500	CFM56
Intake/Engine inlet interface	1	1
Fan inlet	2	2
Fan exit	12.5	13
LPC OGV exit	2.5	2.5
HP Compressor exit	3	3
Combustion section exit	4	4
HP Turbine exit	4.5	4.2
LP Turbine exit	4.9	5

Table 1.3: Thermodynamic stations

When the engine's performance are evaluated, measurements are made at certain locations inside the engine. These locations coincide very often with thermodynamic stations, and the measurements are typically temperatures and pressures, static or total.

1.1.2 Sensed signals

For scheduling power setting systems and trend monitoring, the Electronic Engine Control EEC senses the following pressure and temperature signals. [2][3][4][5]

Fan inlet	P2	T2
LPC OGV exit	-	T2.5
HP Compressor exit	P3	T3
LP Turbine exit	P4.9	T4.9
Fan Exit	P12.5	-

Table 1.4: V2500-A1 - sensed signals

Fan inlet	P12	T12
LPC OGV exit	P2.5	T2.5
HP Compressor exit	PS3	T3
LP Turbine stage 2 inlet	-	T4.95
LP Turbine exit	-	T5
Fan Exit	PS13	-

Table 1.5: CFM56-5A3 - sensed signals

EGT is one of the most essential factors in engine performance studies since it is the most important temperature in the engine's hot sector.

The hot region of the engine has three main temperatures:

- burner exit temperature T4
- HP Turbine exit temperature, identified in T4.5 for V2500 and T4.2 for CFM56
- EGT, identified in in T4.9 for V2500 and T4.95 for CFM56

The burner exit temperature's value of T4 is impacted by the amount of cooling air used by the HPC. Furthermore, it is difficult to install a sensor due to the extreme conditions encountered (high temperature), as these conditions affect the sensor output signal generating sensor biases (systematic errors) which will be discussed in the following chapter.

For the same reasons stated above, the HPT exit temperature is not sensed.

The EGT for the engine V2500 is detected in the LPT exit (station 4.9), but the EGT for the CFM56 is identified in the LP Turbine inter-stage, specifically at the stage 2 inlet.

To do a better analysis of engine condition, some more parameters are potentially accessible for the CFM56 engine in comparison to the V2500 engine: sensor signals

PS13, P2.5, and T5 are used for monitoring the trend of the CFM56 engine in addition to the signals of sensors P12.5, T2.5 and T3 also used for monitoring the trend of the V2500.

Engine condition monitoring is possible by the ability of the FADEC to broadcast the engine parameters through the ARINC 429 bus output.

1.1.3 Details

It is possible to note that both engines have a very identical array of sensors, except for the optional sensors described above for the CFM56.

Both engines are equipped with a resistance probe at the LP compressor exit, going into more detail it is a platinum resistance probe: the operating principle of the sensor is based on the properties inherent to metals (in this case platinum), being that their resistance varies in relation to temperature. Therefore, current supplies to the probe resistor and its signals are modified by the temperature surrounding the probe.

In the other stations, the temperature signals are perceived through thermocouples type K (Chrome (+) - Alumel (-)): the operating principle of the sensor is based on the generation of an electromotive force between two dissimilar conductors, submitted to a temperature gradient.

The thermocouples will be discussed in more detail in the next chapter.

Thermocouples are the most popular sensors used for gas temperature measurements nowadays, owing to their robustness, ease of manufacture, tolerated reaction time, and low cost of use.

Resistance Temperature Devices RTDs are increasingly being used, although each has limitations in size, ruggedness, signal processing, or cost when compared to the more popular thermocouples. Thermistors are not commonly utilized due to their low-temperature range, which is typically less than 200°C, indeed in our references engines are only used in LPC exit.

The greatest difference between the two reference engine was observed in the choice of thermocouple wiring harness design in the station identified as EGT and the transducer type used to read the pressure signal.

Wiring harness design

For the CFM56, nine thermocouple probes are positioned in the T4.95 plane of the LPT stage 2 inlet, which sense and average the EGT.

The T4.95 thermocouple wiring harness, as shown in figure 1.4, has the following elements:

- three identical and interchangeable thermocouple lead assemblies with two probes

- one thermocouple lead assembly with three probes
- one upper extension lead
- one lower extension lead
- one main junction box assembly

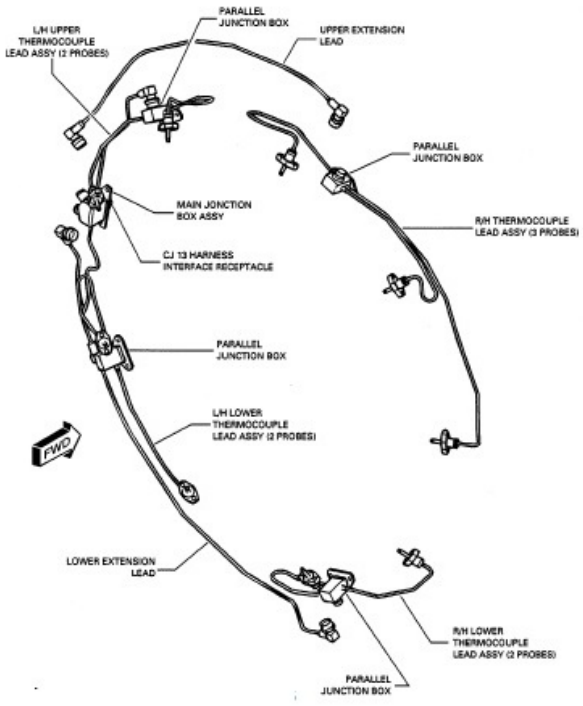

Figure 1.4: CFM56 - EGT Thermocouples Assembly, [4]

The electromotive force is averaged in each individual lead assembly (2 probes and 3 probes), therefore at the level in the main junction box assembly relating to the interface connector, and in a second time, for each individual assembly the averaged electromotive force is sent to the EEC via harness, but the right-side sector and left-side sector lead assembly groups are sent in two different channels.

As regards V2500, four thermocouple probes, in double redundancy, are positioned in the T4.9 plane of the LPT exit, which sense and average the EGT.

There is one main junction box assembly where all the thermocouple lead assemblies are connected and the electromotive force is averaged. Through one connector the average electromotive force is sent to the EEC, but the redundant signal, with respect to the main one, is managed by a different channel, as shown in figure 1.5

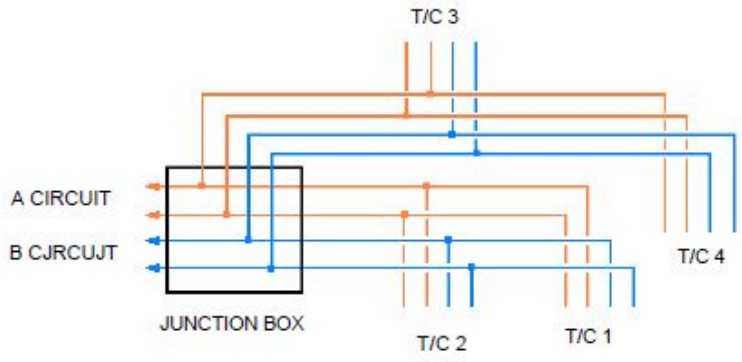

Figure 1.5: V2500 - EGT Thermocouples Assembly, [3]

In way of comparison to the CFM56 engine, the two channels manage different signals but at the same points of the section, while in the CFM56 the two channels manage signals from different points of the section.

Pressure transducer

In the V2500 are installed piezoresistive transducers, silicon capacitive type, while in the CFM56 are installed piezoelectric transducers, quartz capacitive type.

Piezoresistive based transducers rely on the piezoresistive effect which occurs when the electrical resistance of a material change in response to applied mechanical strain. The piezoresistive effect in silicon is due primarily to changes at the atomic level and is approximately two orders of magnitude larger than in metals. When piezoresistors are placed in a Wheatstone bridge configuration and attached to a pressure-sensitive diaphragm, a change in resistance is converted to a voltage output which is proportional to the applied pressure.

Piezoelectric based transducers rely on the piezoelectric effect, which occurs when a crystal reorients under stress forming an internal polarization. This polarization results in the generation of charge on the crystal face that is proportional to the applied stress. Therefore, an electric charge proportional to the applied force is generated when a piezoelectric material is stressed.

In both engines, in each channel is installed a single pressure transducer for each pneumatical line. Consequentially, in the station where there are different rakes mounted in a different positions, the pressure is collected and averaged through a pneumatical line that runs around the section, as shown in figure 1.6.

Figure 1.6: CFM56 - Pressure pick-ups, [5]

The pneumatical line, coming from the engine section within the EEC, through a shear plate is routed to the channel A and B transducers which compute the actual pressures.

Only for the optional monitoring pressures, for the CFM56 engine, the pneumatical lines are supplied by a single channel.

Chapter 2

Signal processing for CFM56 engine

2.1 Full Authority Digital Engine Control - FADEC

Each engine features a FADEC system. The FADEC functions as data multiplexer for the propulsion system, making engine data available for condition monitoring: it provides the engine system regulation and scheduling to control the thrust and optimize the engine operation controlling the fuel flow, the compressor airflow, and turbine clearance.

Furthermore, the FADEC provides over-speed protection for N1 and N2, in order to prevent the engine from exceeding certified limits, and also monitors the EGT.

The FADEC is made up of:

- the EEC containing two identical computers, designated channel A and channel B that cross-talk
- the Hydro-Mechanical Unit HMU which converts electrical signals from the EEC into hydraulic pressures to drive the engine's valves and actuators
- the peripheral components and sensors that are used for control and monitoring

The EEC is the first component of the engine control system and each channel can control different engine system components. Channels A and B are usually always operational but they operate independently from each other: if one fails, the system automatically switches to the other one. The EEC governs the engine in response to thrust command inputs from the airplane and provides information to the airplane for the flight compartment indication, maintenance reporting, and engine condition monitoring.

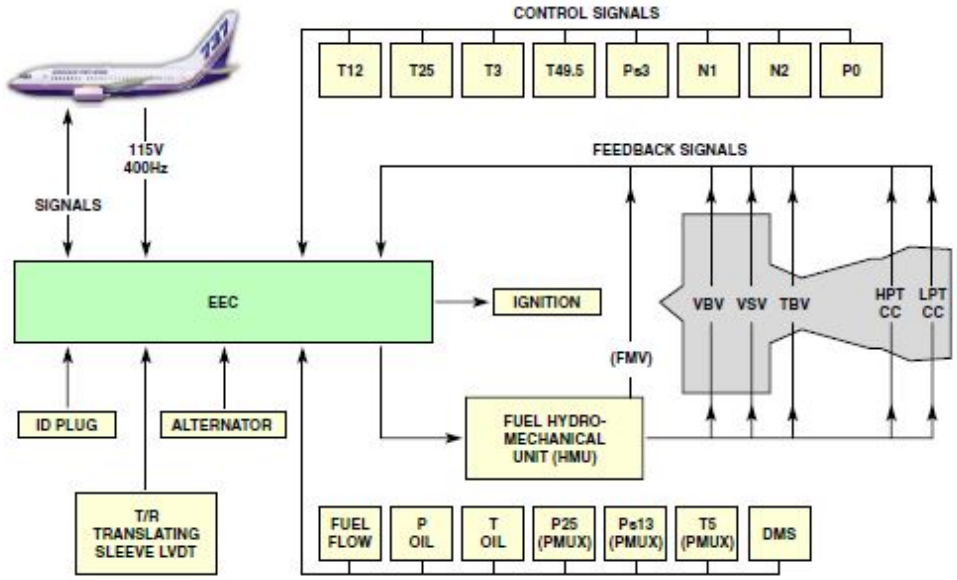

Figure 2.1: CFM56 - control system components, [6]

The EEC receives engine inlet condition data from the Air Data Computers ADCs and operational commands from the Engine Interface Unit EIU.

As shown in figure 2.1, operating condition data from dedicated engine sensors such as T12, PS12, P0, N1, N2, PS3, T25, T3, and temperature case are sent to EEC: through these parameters, it computes the required fuel flow, Variable Stator Vane VSV, Variable Bleed Valve VBV, HPT clearance control, LPT clearance control, and rotor active clearance control valve positions.

The FADEC is categorized as “on condition” equipment which means they are removed only when a failure is indicated.

2.1.1 Signal processing and fault strategy for CFM56

Each channel has all the necessary sensors, engine and aircraft interfaces, a central CPU, and output drivers: the single channel continuously examines and processes its own inputs, and to make sure there are no anomalies, it compares its data with those of the other channels via a cross-channel data link.

The active/stand-by principle is used by the two EEC channels to control their output drivers. This means that while both channels constantly receive and process inputs, only the active channel, also known as ’the channel in control’, delivers control outputs. Active and Stand-by selection is based upon the health of the channels (no fault identified): each channel determines its own health state, and when both channels have an equal health status, the Active/Stand-by channel

selection rotates as each engine starts.

The dual redundant architecture's goal is to lessen the impact of errors in the control system on engine performance.

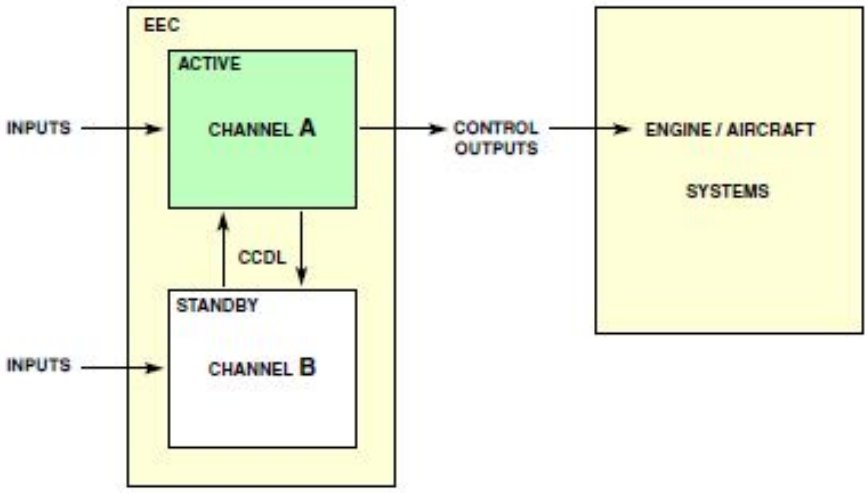

Figure 2.2: EEC Design, [6]

The different inputs from sensors, switches, and aircraft are checked at several stages within the EEC before the values received are finally picked to be used in the control law computations.

After being converted to digital format, the values must go through signal and range check logic to then be compared across the Cross-Channel Data Link CCDL prior to being chosen for the control law calculations.

After the values have been calculated and processed in the control law logic, they pass through the output stage for transmission to the engine, or aircraft systems.

As shown in 2.3, both EEC channels validate their inputs, process the data, and check their outputs identically.

Data validity and range check

When EEC converts parametric analog inputs into a digital representation and subsequently verifies whether the conversion is successful, an internal EEC fault could happen: the signal moves on to the next stage for data validity and range check if it passes the conversion test, therefore if it is considered valid.

With parametric values are meant values that are not fixed but can change within a certain range, as opposed to discrete values, which can only have one of two values, such as on/off or open/closed. The data validity and range test logic receive discrete inputs directly because most of them are treated as digital signals.

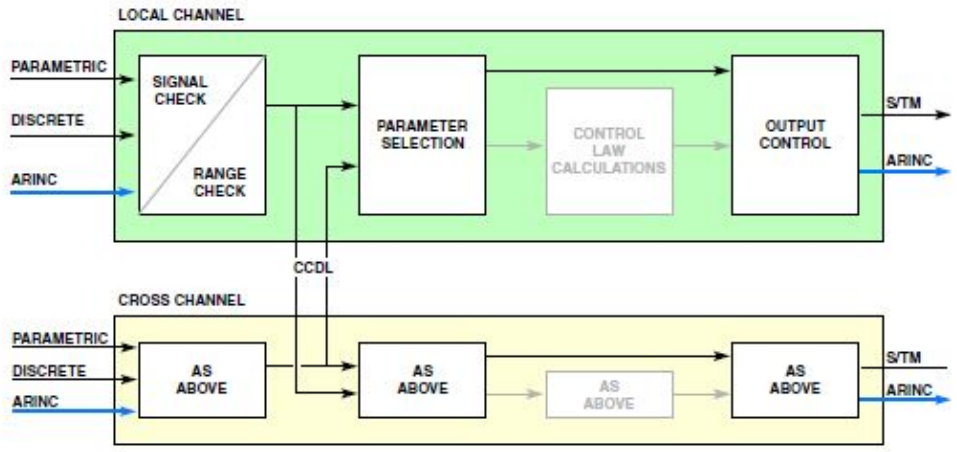

Figure 2.3: Signal processing,[6]

Checking the maximum and minimum bounds against predetermined values is the simplest range test for a parameter and it is used for sensed signals T12, T25 and T5. The EEC then compares the sensor output signal to preset criteria and creates a sensor failure message for the defective channel if:

- the sensed temperature/pressure is not within the maximum and minimum ranges
- the fault persists for more than 4.8 seconds

Although the signal's fault isolation would seem so simple, some inputs take into account other parameters in the calculation phase, making fault isolation more difficult like sensed signal P25, PS13, PS3, and T3. By way of showing, the sensor faults logic for the T3 sensor signal is described: T3 sensor signal is a control input used to calculate the demand on the HPT Active Clearance Control HPTACC valve, in this case, the fault strategy used to isolate the sensor fault is much more stringent because when the engine is running, the EEC checks only the minimum limit, more precisely -60 °C for more than 4.8 seconds, while if the engine is running, the EEC compares if T3 value is less or equal to the selected value of T25, or T3 is sensed as being above 725°C. In both case the error must be present for 4.8 seconds. It is evident that the sensor fault strategy used depends on the operating conditions of the engine.

If the parameter fails the range tests, the EEC sets a flag like 'invalid' and holds the parameter at its last valid value, and the EEC generates an error designed as: '*Signal out of the range*'.

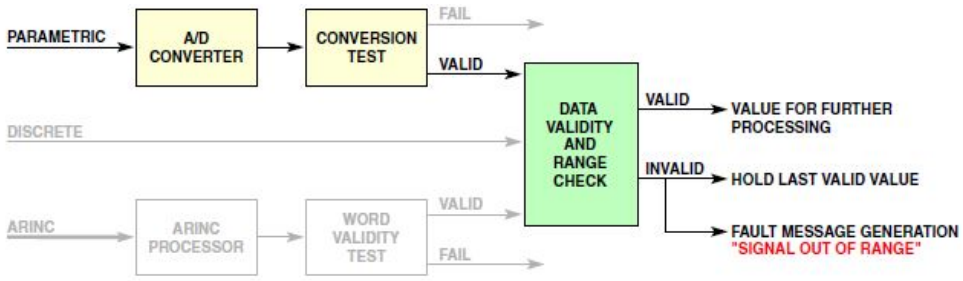

Figure 2.4: Data validity and range check, [6]

Due to all the potential engine failures, isolating sensor faults is not always easy. The logic examples described above, while not giving specific instructions on how to do so, do help understand how challenging it is to isolate sensor errors and how heavily it depends on the engine's control and monitoring logic.

Cross- channel validation

After passing through the signal and range check logic, these values are compared throughout the CCDL: validated input signals and validation status data are sent from one EEC channel to the next via a set of digital discrete control/status signals. This cross-channel data can then be used in the data selection process.

The opposite channel's data is used by the local channel through CCDL if the local channel's digital data is invalid or fails a maximum/minimum range check, provided that the data has passed validity and range tests. If it fails the validation and maximum/minimum range checks also in the stand-by channel, the EEC then chooses either a fail-safe value or, for certain parameters, a model value generated mathematically by the EEC from other parameter values: sensor inputs like PS3, T25, and T3 have an EEC calculated models.

When both channels are operational and cross-channel data is available, the validity of channel A and channel B dual sensor measured values is given by the fact that EEC checks the absolute difference between the two inputs within a predetermined range: if the difference between the inputs is less than the specified tolerance, the average of the values is selected.

The value that is closest to the input model is chosen if the delta between the two inputs is beyond the set range. In the absence of a model for the sensor, a fail safe value is chosen but in either situation, the EEC will produce the following error message: '*Signal disagree*'.

The figure 2.5 schematically summarizes what has just explained above.

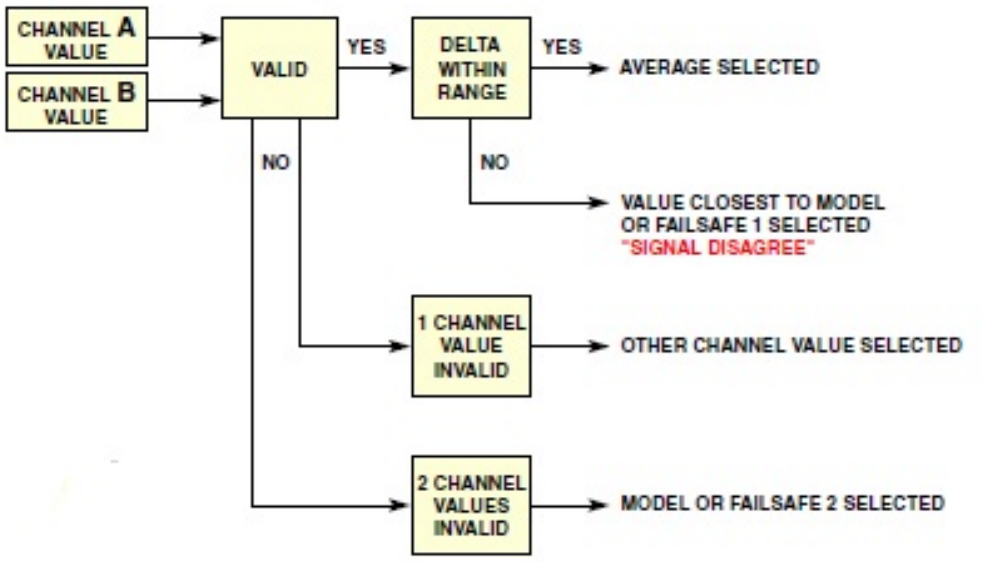

Figure 2.5: Data selection and fault setting, [6]

2.1.2 Range check and Cross - channel validation for EGT inputs

The range check and cross-channel validation for EGT inputs are described as a clarifying illustration.

In the previous chapter, it is highlighted in detail the design of the nine thermocouples that are supplied in the CFM56 engine for the EGT, located in the T4.95 plane of the LPT stage 2 inlet.

The nine probes are grouped to make up four sectors: the right sectors are connected to channel A while the left sectors are connected to channel B.

As long as all sectors are valid, the average value is selected but in the event that one of the sectors is invalid, the selected value is calculated from the weighted average of the valid sectors.

To validate/invalidate the various sectors is implemented an internal logic:

- if the engine is not running, the EEC checks to see if the temperature felt is less than -60°. If a sector's temperature falls below this level, the EEC sets a fault flag and generates an error message'*Signal out of the range*'.
- if the engine is running, the EEC conducts additional examinations on the sectors. If one of the sectors detects a temperature below the specified value of T25 or above about 1300°C, the EEC sets a fault flag and generates an error message. '*Signal out of the range*'.

An error message '*Signal disagree*' is generated by the EEC if one sector has 200°C discrepancy compared to the average of the other sectors.

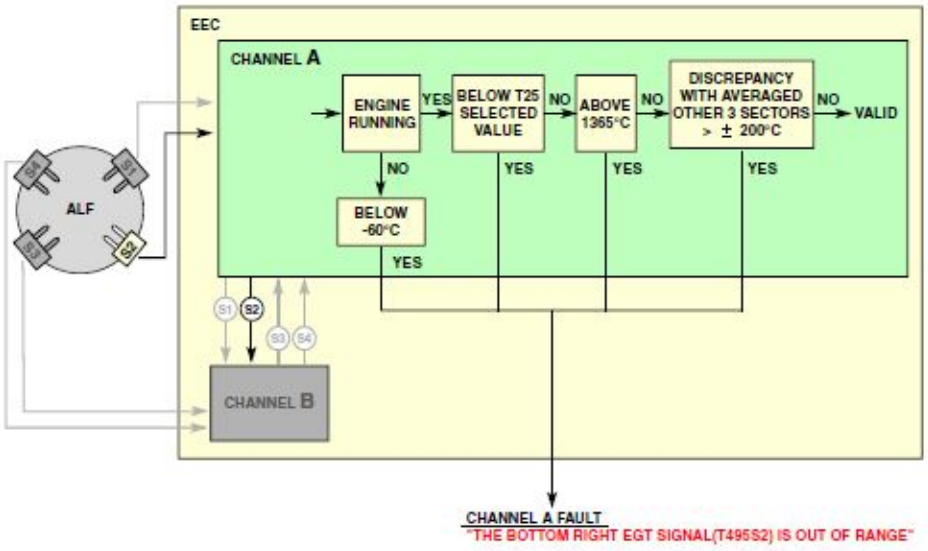

Figure 2.6: EGT signal processing, [6]

There is no true cross-channel validation in the scenario under consideration, since the two channels use separate signals. However, the CCDL performs a discrepancy check in relation to the other sectors.

Chapter 3

Temperature and pressure measurement systems

3.1 Sensor chain

The measurement system should have the capability to accommodate a variety of inputs including both low-level and high-level signals. Typical low-level signals include thermocouples, transducers, and RTDs, while devices such as Linear Variable Displacement Transformers LVDTs produce high-level signals.

In this chapter, it will be discussed only and exclusively low-level signals thermocouples and transducers.

The main elements of a measurement system are the sensor, thermocouples/-transducer, signal transmission/distribution network, signal conditioning, and data acquisition and processing systems.

A schematic representation of the chain for the temperature and pressure measurement systems is provided in figure 3.1 and 3.2.

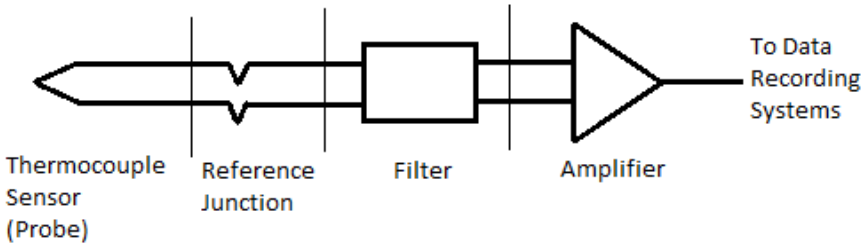

Figure 3.1: Temperature measurement system chain

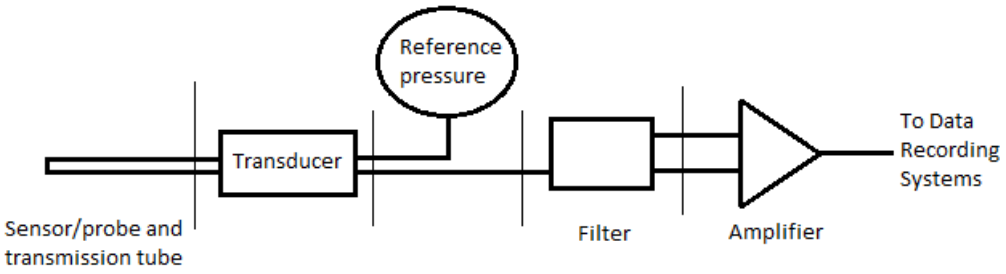

Figure 3.2: Pressure measurement system chain

Data collection and processing systems offer the link between the instrumentation systems and their user's data. These components obtain the outputs from the signal conditioning units and process these electrical signals to generate output data in the specified digital and/or analog formats. This element is identified as EEC. The data acquisition and processing systems have already been thoroughly addressed in the previous chapter.

The intrinsic portion of the instrumentation system for temperature and pressure measuring systems are discussed in details below.

- The sensor is the fundamental element in the hierarchy of a measuring system that takes energy from a physical phenomena and sends it for either a mechanical or electrical transformation to convert the energy into a usable form.

- The thermocouple/transducer is the fundamental link in the measurement system chain and converts the energy of the measure received from the sensor into an electrical quantity that can be amplified and conditioned. These devices are categorized as either active (commonly called "self-generating") because due to a physical input they generate an output without the need of external electrical excitation.

- Any measurement system must have a signal transmission. Simply said, transmission means that measurement can be taken at one physical point, and the signal can then be sent to another location for extra processing, such as signal conditioning or data gathering and processing. The main goal is to convey the necessary information accurately without allowing outside factors to reduce the accuracy of the learned information. In a typical real-time system, signal distribution to the system's various components is accomplished using cables.

- To transform a thermocouple or transducer output into a signal suitable for an input to a data acquisition system, signal conditioning is necessary. The signal conditioning is primarily composed of a filter and an amplifier; the former is used to remove unwanted frequency components or to enhance other frequency components of the signal, the latter provides voltage amplification to normalized inputs to a multiplex system. Since the output is in the millivolt range, amplification of some kind is necessary to increase the amplitude to a level appropriate for further processing.

The connected issues for the two systems, temperature and pressure measurement systems, that are associated with each of the parts mentioned above will then be looked into and highlighted. On the other hand, simply an indication of the related error will be provided for the signal conditioning, the data acquisition and processing systems, which can be neglected.

3.2 Temperature Measurement System

The thermocouple sensor is the initial component in the chain of the temperature measurement system, as shown in figure 3.1.

Usually, the thermocouple sensor consists of the sensing element, the thermocouple itself, surrounded by a stagnation tube, the Kiel head, where the flow velocity is reduced to a level where no further compressibility effects occur and the temperature under total conditions can be measured.

A thermocouple is a device made by two different wires joined at one end, called junction end or measuring end. The two wires are called thermoelements or legs of the thermocouple: the two thermoelements are distinguished as positive and negative ones.

Being a self-generating device, a thermocouple directly produces a voltage that can be used as a measure of temperature. That terminal voltage used in thermometry results only from the Seebeck effect which is due to the association of two physical phenomena: the Peltier effect, or generation of an electromotive force due to contact between two dissimilar conductors, and the Thomson effect, or generation of an electromotive force in a metal bar submitted to a temperature gradient.[7]

The internal electrical potential difference or electromotive force, which is outwardly perceived as a voltage between the terminals of a thermocouple, is known as the Seebeck electromotive force emf. Even if it is not coupled to a circuit, this Seebeck source emf can be found in any electrically conducting substance that is not at a constant temperature. However, for thermocouple thermometry, the net voltage between paired dissimilar materials is always employed due to practical considerations. The Seebeck emf doesn't happen at the thermocouple connections but within thermocouple legs: the emf is generated in the thermocouple wires only in the temperature gradient existing between the "hot" and "cold" junctions and not in the junctions themselves.

The temperature vs voltage relationship is given by:

$$emf = \int_{T_1}^{T_2} S_{12}\, dT = \int_{T_1}^{T_2} (S_1 - S_2)\, dT \tag{3.1}$$

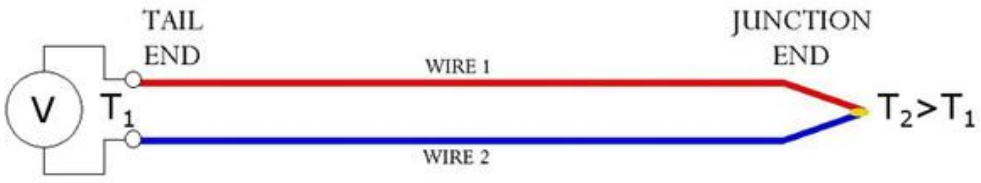

Figure 3.3: Schematic drawing of a thermocouple, [8]

The thermocouple temperature measurement is also a differential measurement because T1 and T2 are being measured at two different thermocouple's stations with T2>T1: a monotonic emf versus junction end temperature T2 relationship, which is the one that is desired, is required to have a usable thermocouple for measurement, ensuring that a distinct voltage is generated at the tail end for each temperature at the junction end. However, from the integral in Equation 3.1, it can be understood that the emf depends on both T1 and T2: a monotonic emf vs T2 relationship cannot be defined if the tail end temperature is not constant since T1 and T2 can change independently.

Only one of them may be unknown. Therefore, the temperature of the measuring junction must be measured according to the known actual temperature of one reference junction. Due to this, the tail end is kept in an ice bath that is created by mixing water and crushed ice reference temperature of 0°C: this reference is used in the rig testing engine.[7]

In the installed engine, the ice bath is typically replaced by an integrated circuit called a cold junction compensator, where the tail end is at a known temperature and temperature fluctuations are tolerated. The voltage of the thermocouple at the tail end can be added to the voltage produced by the cold junction compensator, which is actually equal to the voltage of the thermocouple between 0°C and ambient temperature, to recreate the voltage versus temperature relationship of the thermocouple. A compensating circuit contains a combination of fixed resistors, and a Temperature Sensitive Resistor TSR, which have a similar variation of emf as the temperature of the TSR is varied. If the reference junction of the thermocouple is coupled thermally to the TSR and the compensating circuit is connected in series with the thermocouple, so that its change in temperature/emf opposes to that caused by the reference junction, the thermocouple behaves as if the reference junction temperature were held constant.

In conclusion, with a cold junction compensator, the temperature of the reference junction is allowed to vary, and a compensating emf is introduced into the circuit or accounted for by calculation: the Seebeck coefficient is sufficiently matched to allow the whole instrument's accuracy to be typically 0.25% of full scale throughout a tolerable range of temperatures within EEC.[7]

As shown in the previous chapter, in both reference engines are installed K type thermocouples, which have a range operation until about 1260°C with 3.25 mm wire size like upper temperature limit, and until 760°C with 0.25 mm wire size like upper temperature limit: this range to be considered in a conventional design closed-end protecting tube.

The approximate compositions for positive and negative thermoelements of type K thermocouple are Nickel - 10% chromium (+) versus nickel - 2% aluminum, 2% manganese and 1% silicon (—): approximate compositions because most modern manufacturers now adopt compositions with alterations, which are usually made

to improve the stability and/or manufacturing processing of their wire, that can depart significantly from those of the original formulation.[9]

Large calibration shifts will occur if exposed to a marginally oxidizing atmosphere at a temperature above 800°C due to Green-rot corrosion, such corrosion results from preferential oxidation of chromium when the oxygen content of the atmosphere surrounding the thermocouple is low.[10] This aspect will be explored later.

This thermocouple type presents an accuracy of ± 2.2°C or 0.75% for category 2, while accuracy of ± 1°C or 0.4% for category 1.

Figure 3.4 shows the voltage against temperature relationship for some of the most common thermocouples (letter designated thermocouples) distinguishing positive (P) and negative thermoelements(N): from the graph, it's obvious that for the temperatures inside the reference engines, other thermocouple types could also be installed.

Consequently, it will be clarified why it was chosen type K thermocouple in the reference engines, in accordance with [7]: basically, thermocouples can be divided into two groups: thermocouples with Ni-base thermoelements (type E, J, K, and N) called base-metals thermocouples and thermocouples with Pt-base thermoelements (type R, S and B) called nobles-metals thermocouples.

Type R, S, and B thermocouples employ Pt-base thermoelements and can withstand temperatures of up to 1700°C; however, they are more expensive and have a lower voltage output than type K. Ni-based thermocouples, on the other hand, can operate at lower temperatures than Pt-based thermocouples, but for the engine taken as reference, the temperature range, at which the two types of thermocouples can operate, does not affect the choice. The main difference that influenced the choice is that the continued use of Types R and S thermocouples at high temperatures results in excessive grain growth, which can lead to mechanical breakdown of the platinum element, resulting in less durability than type K thermocouples.

As regards thermocouples with Ni-base thermoelements, the only two thermocouples with Ni-base thermoelements that can be ruled out are type J and type E, the former because the rate of oxidation of the iron thermoelement (positive thermoelement) is rapid above 540°C, and the use of heavy-gauge wires is recommended when long life is required at higher temperatures, the latter because type K oxidation resistance characteristics are better than type E.

Regarding type N thermocouple, it works well with reference engines because it varies from type K because it has silicon added to both the NP and NN wires as well as more chromium in the NP wire. The NN wire also contains roughly 0.15% magnesium. This thermocouple offers lower drift rates around 1000°C, does not exhibit the short-range ordering of type K materials and is less vulnerable to preferential oxidation effects compared to type K thermocouples.

Between the measuring junction and the reference junction extension wires are

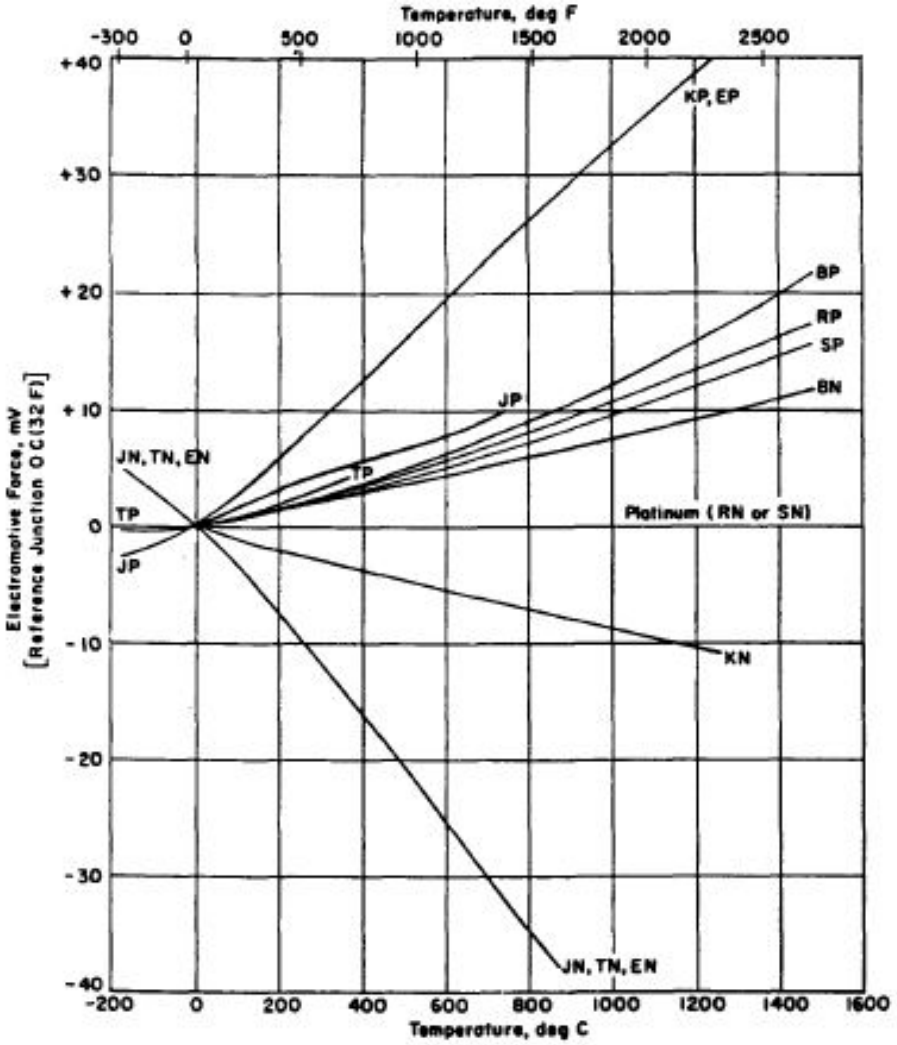

Figure 3.4: Thermal emf of thermoelements, [7]

inserted, which have nearly identical thermoelectric properties as the thermocouple wires they are used with. Some advantages of using extension wires are:

- improvement in mechanical or physical properties of the thermoelectric circuit
- thermoelectric circuitry cost reduction. For instance, in cases when the reference junction is located far from a noble metal, some base metal extension wires may be used in place of noble metal wires thermocouple
- interchangeability of the thermocouple without having to replace the entire thermocouple chain

Assuming that an extension wire category 1 was employed in the thermocouple design stage, which means alloys identical to those used in thermocouples, there are various potential sources of temperature measurement inaccuracy in the use of extension wires in thermocouple circuits.

The main source of mistake can occur if there is a temperature difference between the two thermoelement-extension wire junctions: an undesired emf will occur across the two junctions.[7] [11]

This Δemf will be perceived as an error in the thermocouple output that is being measured. For every degree of ΔT between the thermocouple-extension wire junctions, such errors do not exceed approximately one degree at the measurement junction. Equilibrating the two junctions' temperatures, this means isolating the thermoelement-extension wire junctions part carefully, the inaccuracies will be eliminated.

3.2.1 Mineral Insulated Metal Sheathed - MIMS

The simplest thermocouple is constructed from two thermoelements linked at one end and left directly exposed to the operational environment's atmosphere. The working environment may be an oxidizing, reducing, or inert atmosphere, and using thermoelements in certain of these environments may be restricted due to incompatibility between the materials used to make the thermoelements and the gases, which may cause rapid deterioration. For instance, green-rot corrosion in type K thermocouples due to oxidizing atmospheres in temperatures above 800°C.

The Mineral Insulated Metal Sheathed MIMS configuration can solve the issues caused by the interaction of thermoelements with the atmosphere: the thermoelements are shielded from the environment by a metallic sheath, that provides mechanical protection, and a ceramic material provides electrical insulation between the thermoelements and the sheath.

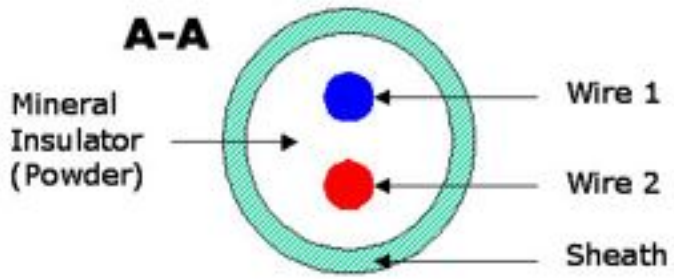

Figure 3.5: Mineral Insulated Metal Sheathed- MIMS, [8]

Although in a MIMS thermocouple the thermoelements are working in the environment made by the insulator and the sheath, the interaction with the insulator and the sheath may affect the stability of the signal and cause drift.[12]

The major functions of the sheath material are to keep the ceramic compact, shield the thermoelements and ceramic from the environment, and offer the assembly mechanical strength.

Sheathed thermocouples often use magnesium oxide as the insulation material. Magnesium oxide is a widely used thermocouple insulator due to its general compatibility with common thermoelements and sheathing materials, as well as its accessibility, reliability, and cheap cost.

The thermoelement's properties are identical to those of other thermocouples described above but, since they are contained in a protective sheath, therefore, small diameter wires can be subjected to high temperatures for longer than the bare wire of the same size with less damage, provided they are constructed and sealed appropriately.[10] [12]

Although MIMS configuration can provide wire protection, the time response of MIMS thermocouples to changes in the operating environment's temperature is slower than traditional bare wire configurations. The MIMS with an exposed Bare Wire Junction configuration can solve the issues: in this type of junction, the sheath and insulating material are removed to expose the thermocouple wires exposed for a specific length, as shown in figure 3.6.This cause the wires are subject to mechanical damage because are exposed to the environment while the thermocouple will have a fast response.

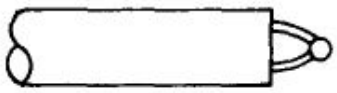

Figure 3.6: MIMS thermocouple with exposed Bare Wire Junction,[7]

A thermocouple's response time is typically defined as the time taken for the thermal voltage (output) to reach 63.2% of maximum for the step change temperature in question, and this corresponds to the time when the temperature difference between the thermocouple and the environment has been reduced by $e^{-1}(36.8\%)$ of the initial difference.

The response time is affected by a number of factors, including thermocouple dimension, construction, tip configuration and the nature of the medium in which the sensor is placed.

To provide an order of magnitude, typical thermocouple response times are shown in table 3.1.

Sheat outside diameter	**Junction type**	**response time [s]**		
		250 [°C]	430 [°C]	850 [°C]
6.0 mm	insulated	4	5	16
	exposed	0.4	0.5	0.16
3.0 mm	insulated	1.1	1.4	4.5
	exposed	0.11	0.14	-
1.0 mm	insulated	0.18	0.21	0.73
	exposed	-	-	-

Table 3.1: Typical thermocouple response time

For exposed measuring junctions, the thermocouple response time is about 10 time less. With conductor diameter in the range 0.025mm to 0.81mm, response times in the region of 0.05 to 0.40 seconds can be realised.[13]

The transient response time of a thermocouple can be defined from a first order, linear differential equation that results from the heat balance between the thermocouple and the surrounding fluid.[7]

The thermocouple energy balance, neglecting thermal radiation transport, balances the thermocouple convective loss with the time rate of change in the thermocouple stored energy.

$$hA\left(T_e - T\right) = mc\frac{dT}{dt} \tag{3.2}$$

Where:

- m = thermocouple mass
- c = specific heat capacity of the thermocouple material
- h = heat transfer coefficient
- A = thermocouple heat transfer surface area

Eq. 3.2 is rewritten in the form of a first-order ordinary differential equation.

$$\tau\frac{dT}{dt} + T = T_e \tag{3.3}$$

Where the time constant, τ, for thermocouple is defined as:

$$\tau = \frac{mc}{hA} \tag{3.4}$$

The thermocouple temperature can be solved as a function of time for the immediate change in fluid temperature at time zero:

$$T = Ce^{\frac{t}{\tau}} + \frac{1}{\tau}\int_0^t T_e e^{\frac{-t}{\tau}} dT \tag{3.5}$$

Where:

- T = thermocouple temperature
- C = integration costant
- t = time
- T_e = environment temperature

Figure 3.7 shows the transient response of a thermocouple. While 63.2% of the final temperature is reached after one time constant, it takes 5τ for the value to reach 99.3% of the new temperature value.

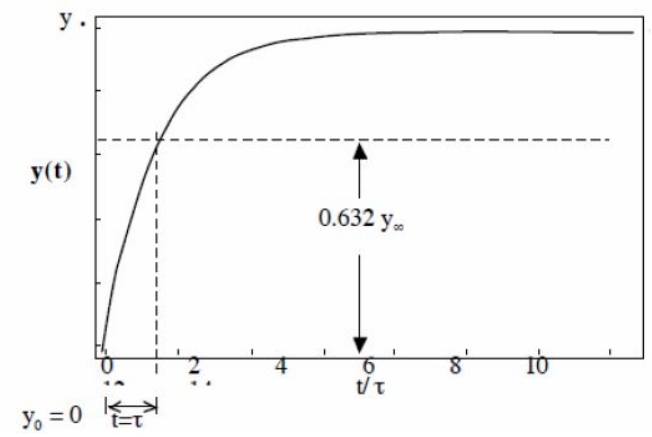

Figure 3.7: Transient response of a thermocouple, [7]

3.2.2 Error source: BIAS thermocouples

Sensing elements have limitations that must be understood in order to ensure measurement accuracy. This accuracy will be determined not only by the sensing element itself, but also by the design of the probe into which it will be inserted. As a result, the probe design will always be a compromise between the probe dimensions limited by available space, strength criteria, and the best possible aerodynamic probe characteristics to meet the required measurement accuracy.

The aim of the thermocouple probe design is to produce an environment that allows the thermocouple to measure gas temperature with the required accuracy.

Temperature readings from thermocouples junction, T_J, submerged in flowing gas via the walls of a gas duct, differs from the total temperature of the gas, T_T, which is the thermodynamic parameter relevant to the engine. T_J is the result of thermal equilibrium between the thermocouple and the surroundings environment.

According with [11] and [14], the most important thermodynamic factors affecting thermocouple probe design are:

- conduction along the wires and the sheath of the thermocouple
- radiation to/from the walls and the blades/vanes surfaces
- convection at the boundary layer around the thermocouple

Figure 3.8 shows the schematic cross-section of such a sensor design with the basic heat transfer phenomena indicated above.

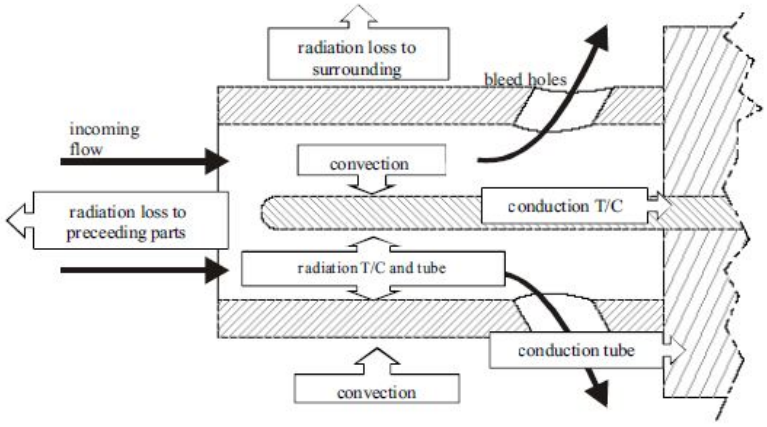

Figure 3.8: Schematic cross-section of total temperature sensor,[14]

Conduction and radiation cause two types of measurement errors: conduction error and radiation error.

Furthermore, getting the total temperature of a flowing gas is required in order to transform the kinetic energy of the flowing gas into a temperature increase, which means to stop the gas adiabatically, In practice, this is only an ideal process: as a result, the measured total temperature at the thermocouple junction T_J shows to be lower than the actual total temperature T_T of the gas. A measurement error arises, called velocity error.

Summarizing, aerodynamic and thermodynamic factors generate three types of systematic errors in thermocouples:

- velocity error
- conduction error
- radiation error

The errors mentioned above will be discussed detail, in according with [11], [14] and [15].

Velocity error

The difference between the total temperature of the thermocouple junction T_J, and the total temperature of the gas T_T, is described with the so called recovery factor R and is defined as:

$$R = \frac{T_j - T_S}{T_T - T_S} \tag{3.6}$$

This is the ratio of the actually measured to the total thermal energy available from the flow's adiabatic deceleration.

A good thermocouple design is achieved if the recovery factor is very close to 1. The recovery factor R of a bare wire thermocouple is a function of the thermocouple geometry and can be varied only between narrow limits. For bare thermocouple wires recommended values of R for probe designs are:

$$R = 0.68 \pm 0.07 \; wires \; normal \; to \; flow \tag{3.7}$$

$$R = 0.86 \pm 0.09 \; wires \; parallel \; to \; flow \tag{3.8}$$

Due to the incomplete deceleration, a velocity error remains that can give as:

$$Y_v = T_T - T_J = (1 - R) \frac{\frac{\gamma-1}{2} Ma_J^2}{1 + \frac{\gamma-1}{2} Ma_J^2} T_T \tag{3.9}$$

The Mach number inside the Kiel at the thermocouple junction Ma_J is extremely important in velocity inaccuracy: this Mach number strongly depends on the free-stream Mach number Ma_F.

Being the free-stream Mach number Ma_F an engine parameter, the only way to alter the thermocouple junction Mach number Ma_J is to change the area ratio of the Kiel head intake AE and exit bleed holes AB.

$$Ma_J = \frac{Ma_F}{\frac{AE}{AB}} \left(1 + \frac{\gamma - 1}{1} Ma_F^2\right)^{-\frac{1}{\gamma-1}} \tag{3.10}$$

In conclusion, the velocity error can be increased, or reduced, by changing the internal flow Mach number Ma_J, regulating the inlet-to-exit area ratio: a higher inlet-to-exit ratio minimizes velocity error.

The variation of thermocouple junction Mach number Ma_J concerning Kiel entry AE, to bleed hole AB, area ratio, for different free-stream Mach number Ma_F is shown in figure 3.9

On design, in practical cases, is prudent to keep Ma_J between 0.05 and 0.15 to minimize the velocity recovery error.

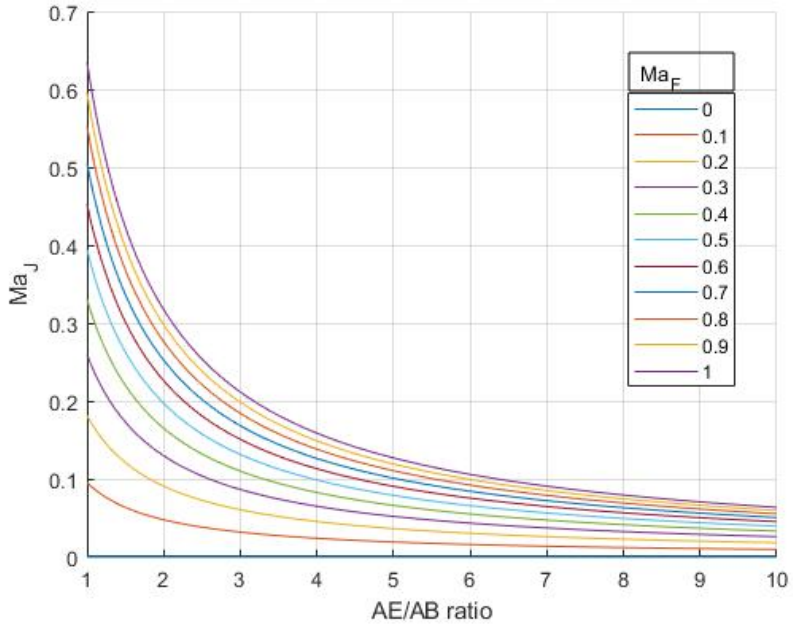

Figure 3.9: Dependence of the Ma_J to AE/AB ratio

The aerodynamic recovery factor R can be used in conjunction with the overall recovery factor, which serves as a measure of how well the total temperature probe under test recovers the total thermal energy of the flow, to perform a correction factor Δ.

This correction factor Δ is defined in equation 3.11 and is related to the aerodynamic recovery factor and ratio of static to total temperature. This correction factor is subsequently added to the overall recovery factor defined in equation 3.12 to give the flow total temperature through the corrected recovery factor $\bar{R}$ in equation 3.13.

$$\Delta = (1 - R) \left(1 - \frac{T_S}{T_T}\right) \tag{3.11}$$

$$r = \frac{T_J}{T_T} \tag{3.12}$$

$$\bar{R} = r + \Delta = r + (1 - R)\frac{\frac{\gamma-1}{2}Ma_F^2}{1 + \frac{\gamma-1}{2}Ma_F^2} \tag{3.13}$$

This corrected recovery factor $\bar{R}$ is used to correct errors due to Mach number effects.

Conduction error

It is assumed that the heat energy transferred from the hot gas to the thermocouple hot junction through forced convection is equal to the heat energy transferred through conduction along the thermocouple wire. The thermal energy loss due to conduction is given by the following equation:

$$Y_c = T_T - T_J = \frac{T_T - T_M}{\cosh\left[L\left(\frac{4}{D}\frac{h_c}{k_S}\right)^{\frac{1}{2}}\right]} \tag{3.14}$$

Where:

- T_M = mount temperature
- L = length of thermocouple exposed
- D = wire diameter
- h_C = convective heat transfer coefficient
- k_S = thermal conductivity of thermocouple material

The conduction error Y_c is determined by the temperature differential between the gas and the probe wall, the L/D ratio of the thermocouple, the convective heat transfer coefficient h_C, and the thermal conductivity of the thermocouple material k_S.

It is reasonable to consider as fixed the mount temperature T_M and the thermal conductivity of thermocouple k_S, because the first one is determined by the action of the external environment on the support and stagnation tube structure, and the designer can control the effects of the duct wall temperature by insulation between probe and duct wall, while the second one depends from the material of the thermocouple.

What has been said leads us to conclude that the only way to increase, or reduce, conduction error is a variation of the convective heat transfer coefficient h_C or L/D ratio.

The convective heat transfer coefficient h_C is calculated from the Nusselt number Nu which in turn is calculated from the Reynolds number Re.

$$h_C = \frac{Nu\ k_g}{D} \tag{3.15}$$

The Nusselt number can be evaluated through empirical equation:

$$Nu = (0.44 \pm 0.06)\ \ Re^{0.5}\ wires\ normal\ to\ flow \tag{3.16}$$

$$Nu = (0.085 \pm 0.009)\ \ Re^{0.674}\ wires\ parallel\ to\ flow \tag{3.17}$$

Where

$$Re = \frac{\rho \, V \, D}{\mu} \tag{3.18}$$

It is possible to notice that a possible strengthening of the convective heat transfer coefficient is directly coupled with a higher flow velocity inside the sensor, which returns as a counterpart increases in the velocity error.

The figure 3.10 illustrates the effect that the ratio L/D can have on conduction error for a thermocouple normal to flow.

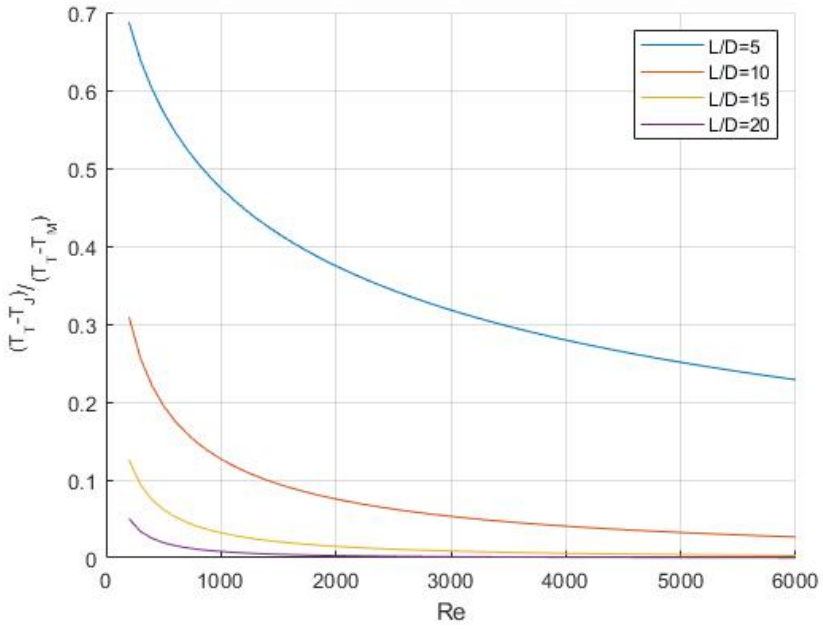

Figure 3.10: Effect of the L/D ratio on conduction error

In conclusion, the conduction error can be increased, or reduced, by changing the heat transfer coefficient h_C or L/D ratio: a higher h_C reduces the conduction error at the expense of the velocity error because a higher h_C corresponds to an increased thermocouple junction Mach number Ma_J, in the worst case, while a higher L/D ratio minimizes the conduction error. Another way to have higher h_C to reduce the conduction error is a smaller wire diameter.

Radiation error

Due to the flow slowdown towards the total condition, the thermocouple is at a greater temperature than the adjacent components: the stagnation tube has a temperature near the static temperature due to a large heat transfer to the free stream. Furthermore, due to flame radiation or excessive air cooling, the engine parts in front of the sensor may have a greater or lower temperature.

This results in a significant radiation heat transfer that can be expressed by:

$$Y_r = T_T - T_J = \frac{1}{h_c} \frac{\sigma \epsilon}{1 + \frac{A_{TC}}{A_W} (1 - \epsilon)} \left(T_T^4 - T_W^4 \right) \tag{3.19}$$

Where:

- σ = Boltzmann constant = 5.67 10^{-8} $W/(m^4 K^4)$
- ϵ = emissivity of thermocouple = 0.2
- T_W= wall temperature
- A_W = wall surface

Other than h_C, all other parameters are fixed. The only way to increase, or reduce, the radiation error is by changing h_C: a higher h_C reduces the conduction error but corresponds to an increased thermocouple junction Mach number Ma_J, which, as seen for the conduction error, implies an increase of velocity error.

The emissivity ϵ is basically fixed by the thermocouple material, but it changes during engine running in an unpredictable way due to oxidation or deposition.

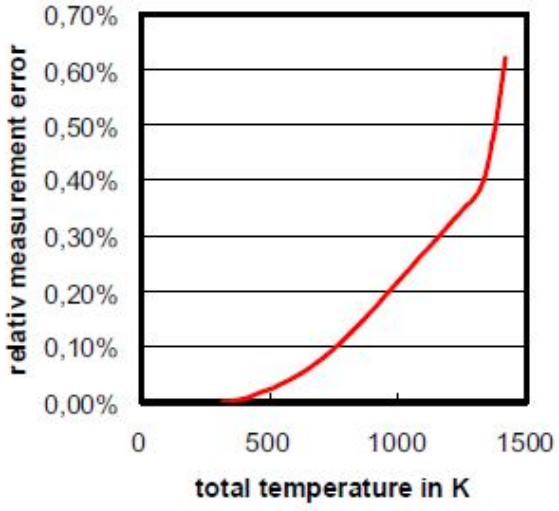

Figure 3.11: Error due to radiation heat transfer, [14]

Figure 3.11 illustrates the influence of the radiation heat transfer. It is clear that radiation has an impact on temperature starting at about 500K. This effect becomes noticeable around 1000 K, even when compared to other errors like the thermocouple error. The assumption that the maximum temperature of all engine components is constrained, results in a significant change of the gradient around 1300 K. Above this point, the surfaces immediately around the sensor will be cooled and the temperature difference will increase. As a result, the radiation heat transfer has risen sharply.

Another type of radiation is radiation error induced by gas and flame radiation, but is generally considered to be negligible at atmospheric pressure and temperatures experienced in the gas turbine.

3.2.3 Error source: Aging/Drift and Inhomogeneities of the thermocouple

When a thermocouple is used to measure an environment's temperature, it is expected that the obtained voltage will remain constant if the environment's temperature is constant. Even though the environment's temperature remains constant, the voltage might actually fluctuate over time; this phenomenon, known as drift, is a source of mistakes in thermocouple measurement and generates a decalibration of the thermocouple.

The decalibration can be caused by changes in the metallurgical state of the thermocouple materials or in the composition of the thermoelements:[7] [10] [12]

- metallurgical changes can be caused by mechanical deformations of the thermoelements, the annealing procedure, or solid-state phase deformation
- the composition changes may be caused by reactions between the thermocouple wires and the insulation, by impurities in the gases surrounding the wires or impurities from the sheath

According to [10] [12], the main phenomena responsible for type K thermocouple drift are oxidation and short-range order transformations.

According to [7], short-range ordering contributes to drift in the temperature range of 200-600°C. On the contrary, oxidation becomes considerably above 800°C. As a result, it can be assumed that sections of the thermocouple below 600°C are primarily affected by short-range order and sections above 600°C are primarily affected by oxidation: this approximation allows to decouple the contribution to drift from oxidation and short-range order transformation, as shown in figure 3.12. These approach is confirmed in [10]

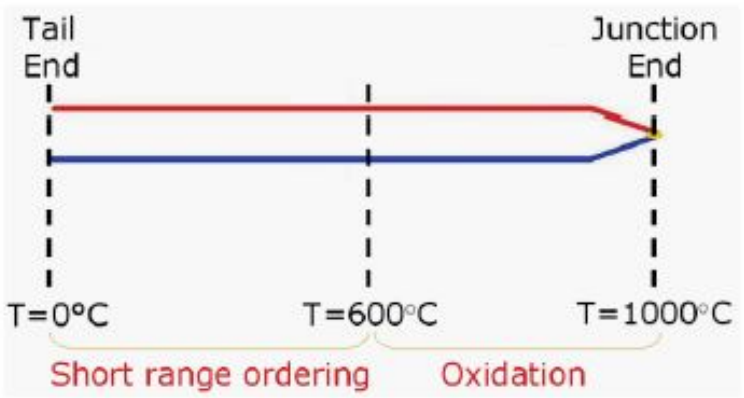

Figure 3.12: Sections of the thermocouple affected by short range order and oxidation, [10]

- Oxidation: when type K bare wires thermoelements are exposed to air, they oxidize. Above about 800°C the effect of oxidation on Ni alloys becomes important. The oxidation produces an extensive change in composition as a result of the formation of oxide scales on the surface of the thermoelements.

  By way of showing, it is considered the effect of oxidation on the positive thermoelement KP (Ni-Cr alloy). In the positive thermoelements KP, Cr is oxidized preferentially forming Cr-rich oxides. The Cr content of the alloy is not enough to form a continuous external chromium oxide, so an external Ni oxide is formed with an underlying Cr rich oxide layer.

  Because Cr is depleted from the base metal in order to generate Cr rich oxides, the Cr oxide has a higher Cr concentration than the alloy. As a result, the Seebeck coefficient is reduced, causing drift.

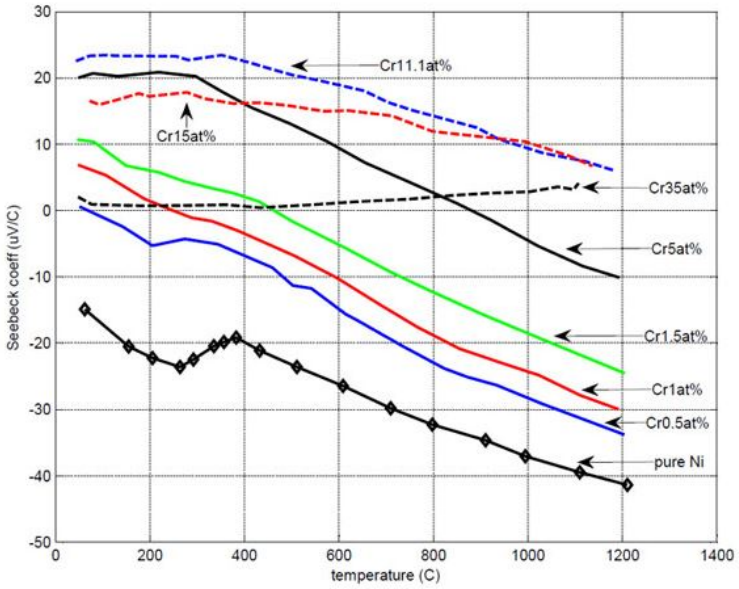

Figure 3.13: Effect of Cr on the Seebeck coefficient of Ni, [8]

- Short-range order effect: in general, the phenomenon arises because, in the range of temperatures between 200°C and 600°C, the elements of the KP thermoelement, locally developed ordered atomic arrangements. The exposed part becomes heterogeneous causing an increase in the Seebeck coefficient.

  The Seebeck coefficient change is time-dependent, and at each temperature, it increases until a maximum value, which is identified at about 400°C. For higher temperatures, it decreases, up to regenerating the disordered structure of the KP thermoelement for temperatures above 600 °C.

As a result, it may be stated that the Seebeck coefficient changes reversibly as a result of the crystal structure's short-range ordering.

The rate of these changes is affected by a variety of factors, including the temperature, the composition of the thermoelements, the composition of the surrounding elements, and the size of the thermocouple wires.

Both, low-temperature and high-temperature, phenomena impacting the Seebeck coefficient need to be considered to account for drift:

$$emf = E_0 + \Delta emf_{short-range} + \Delta emf_{oxidation} = \int S\frac{dT}{dx}dx \tag{3.20}$$

A change in the Seebeck coefficient is a necessary condition to have drift, but it is not a sufficient condition for it because the change in the Seebeck coefficient needs to occur in a region of temperature gradient according to the equation 3.20.

In the MIMS with exposed bare wire junctions configuration, the only thermocouple part subjected to oxidation is the junction, being the only part of the thermocouple exposed to the surrounding environment.

But changes at the junction of the thermocouple usually do not play any role in drift because it can be assumed that the junction is at a constant temperature.[8]

For this reason, only the change caused by the short-range order effect contributes to drift in the MIMS with exposed bare wire junctions configuration.

According to [12], the behavior of the MIMS thermocouple is very similar to a type K bare wire thermocouple tested in a low oxygen content atmosphere, which is affected only by short-range ordering, once the effect of oxidation is removed. This confirms that at 1000°C for MIMS thermocouples the short-range order is the main drift contribution, and the drift curves, in figure 3.14, can be used to estimate drift.

The only remaining potential cause of drift is the interaction with the sheath, but for the same reasons that the contribution of oxidation to drift is neglected, it will not be taken into consideration.

Drift curves for positive KP thermoelement and negative KN thermoelement at 600°C, 800°C, and 1000°C are shown in Figure 3.14: these drift curves are obtained in a low-oxygen content atmosphere to simulate only the short-range order effect.

In figure 3.14, short-range order effects are evident even for temperatures above 600°C: the exposition of the junction of a type K thermocouple at a temperature above 600°C brings a portion of the positive thermoelement to undergo the short-range order transformation and drift will take place.

The contribution to drift from the KP thermoelement is predominant with ranges between +100 and +120 μV after 400 h exposure. As temperature increases, a decrease in KP drift occurs. The contribution from KN thermoelement is between +5 and +15 μV but no temperature dependence can be detected for KN thermoelement.

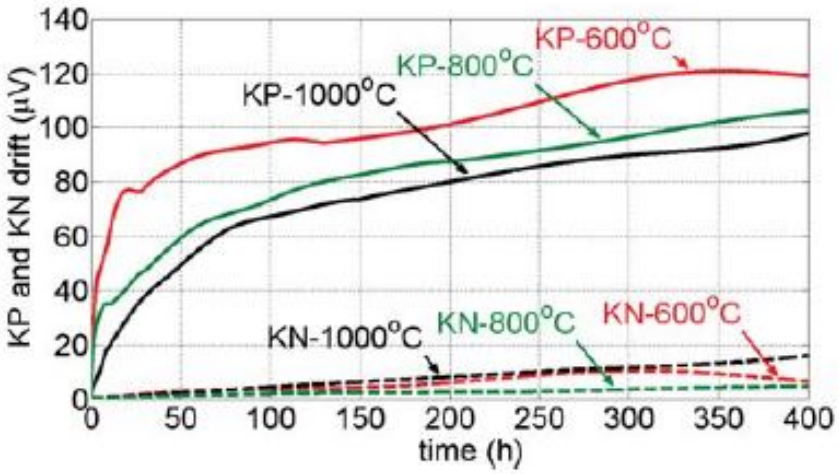

Figure 3.14: Drift for bare wire KP and KN thermoelements (3.2 mm wire diameter) in low oxygen content atmosphere - short-range order effect, [10]

As a result, it may be confirmed that the KP thermoelement is the primary cause of drift between 0 and 600°C, based on evidence of a short-range order transformation in the KP thermoelement, well documented in the literature.

3.2.4 Other error source

The most common types of thermocouple damage that set the stage for a sensor fault are:[16]

- missing probe tips, which is potentially the most serious condition of all from the standpoint of the possible effects on the control system. In this case, the probe tip is completely missing from the affected thermocouple.

Figure 3.15: Missing probe tips, [16]

If the thermocouple is inserted directly in the flow, the thermocouple is

subjected to foreign object damage, whatever the damage that separated probe tip may inflict on another part of the engine on its way through the turbine. The presence in the system of a thermocouple without a probe tip has a marked effect on the average temperature signal, such that the complete loss of the thermocouple can be considered.

- open sensor circuits, which occur when a thermocouple develops an open circuit, which generally occurs adjacent to the weld point of the two thermoelements in the sensing element.

Such damage can occur if, for example, hot spots develop in the turbine inlet because of improperly functioning fuel nozzles. Hot spots in this location can cause a dramatic increase in erosion and sulfidation of metal surfaces, which greatly reduces the service life of thermocouples.[17]

Also that even under the best of conditions, the effects of heat, erosion, and sulfidation will eventually exact their toll on all thermocouples. This is why thermocouples should be inspected at regular intervals.

When a thermocouple develops an open circuit, it generally occurs adjacent to the weld point of the two thermoelements in the sensing element.

3.2.5 Maintenance

Due to the fact that the manuals for the two reference engines are not available, the following chapter summarizes the information provided by the *Operation and Maintenance Manual* for Allison 250-C18.[18]

Temperature measurement system maintenance consists in inspection and replacement of the thermocouple assembly.

The inspection consist in two phases:

- visual check
- electrical check

The visual check is executed through a strong light and 10X magnification to identify wear, broken leads or other damage. The inspection of the thermocouple tip is vital to identify cracks, erosion, and scale.

Thermocouple assembly will be replaced for any of the following reasons:

- excessive wear or damage to the leads
- probes or tips that indicate melting or show other evidence of over-temperature
- tips which evidence erosion to the point that either wire has been reduced in area an estimated 25% or more

- tips having scale on either wire affecting 25% of the cross-sectional area. If the thermocouple is otherwise satisfactory, it is possible to remove the scale by soft grit blast.

The electrical check of the thermocouple assembly consists in a continuity check and an insulation check.

The continuity check has to be carried out in order to determine the resistance of the thermocouple. An open circuit in the harness assembly will cause this resistance to be high, while a short circuit will cause it to be low.

The insulation check has to be carried out acceptable resistance to ground. In presence of carbon buildup on the probe tip, it causes a short to ground, therefore resistance to ground is less than the minimum acceptable. In this case, it is necessary to clean carbon deposits from the probe using a clean soft cloth or by salt/grit blast.

Low resistance can be caused by carbon formation on the probe tip, but also by oxide insulation shorting the probe to ground.

Furthermore, special inspections are scheduled in case of over-temperature operation or hot start encountered.

Because thermocouple types, temperature ranges, construction, application, and intensity of use are so numerous and varied, there are no formally specified frequencies for recalibration. To meet its requirements and experience, an in-house quality management scheme should evolve a checking and recalibration program. Where thermocouples are installed for an extended period of time, calibration checks are best performed in-situ by allowing for the insertion of a standard alongside the working thermocouple, in alternative a thermocouple can be substituted for a standard thermocouple and their emf compared.

A change in the emf and calibration of a thermocouple as the result of use, or even as the immediate result of calibration, can be quantified by immersing the thermocouple in a thermally stabilized bath or furnace held at an appropriate temperature and measuring the output at a series of immersion depths spanning the normal working depth. If the thermocouple is substantially over-immersed, i.e. beyond any previous working depth, the measured emf should closely approximate the value shown on the (first) calibration certificate at the corresponding temperature, therefore the calibration system is validated.

For base-metal thermocouples, a replacement with a calibrated thermocouple rather than a recalibration is often the best solution. In practice, a periodic replacement program may be preferable.

3.3 Pressure Measurements System

The probe is the initial component in the chain of the pressure measurement system, as shown in the figure 3.2.

There are many probe types available in the market but only a limited number of them can be used in turbomachinery due to the presence of various constraints that make this field very demanding in terms of robustness and frequency response. Especially in fully unsteady environments, fluctuations and turbulence amplitude, frequency, and vortex scale are the most crucial factors to consider in order to safeguard a steady-calibrated probe submerged in a fully unsteady environment from reading an untrue pressure.

The most popular probe is the Pitot device, through which the dynamic pressure, which is the difference between stagnation pressure, recorded through the probe intake, and the static pressure, captured by lateral holes not exposed to the main flow stream, may be measured. Although due to the limited ducts' section in which they have to be installed, there is the need to miniaturize the probe, then separate total and static tubes have to be harnessed.

A flow misalignment, even a slight deviation, can produce a significant mistake in total pressure reading in this type of probe, therefore is used to get a flow field measurement almost parallel to flow direction, the direction along which the probe error is null.

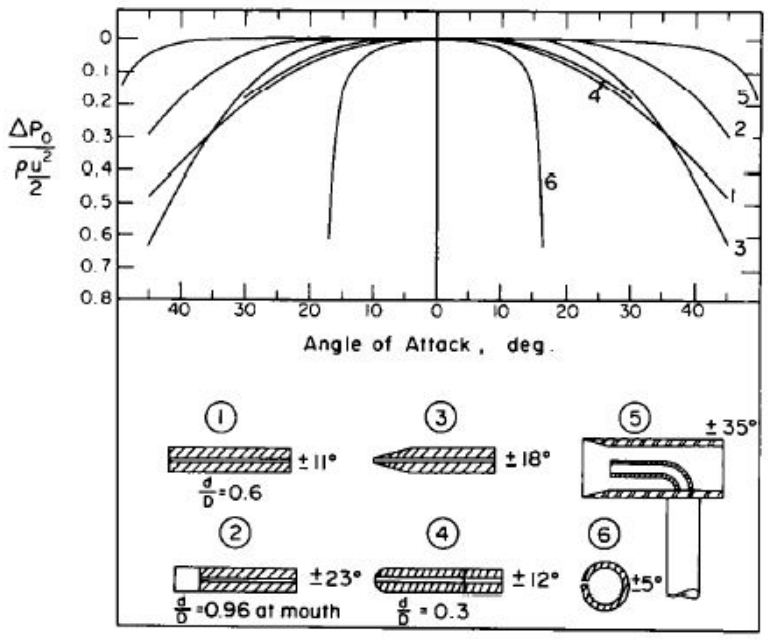

Figure 3.16: A comparison among different probes' insensitivity ranges, [19]

The study carried out by Chue [19] provides an important conclusion that supports the claim that even though there are various Pitot probe designs, each with a distinct yaw angle insensitivity range, they all have considerably lower critical insensitive angles than Kiel-head probes, making Pitot probes unsuitable for highly unstable environments.

The critical angle is the incidence, referred to either yaw or pitch, at which the stagnation pressure error overtakes the amount of 1% of the pressure measured at a null angle of attack.

The Kiel-head probe is nothing more than a Pitot probe whose intake is protected by a shroud, and it is helpful to obtain stagnation pressure because of the extremity probe that derives from the Pitot probe.

It can be used if the probe axis alignment and the flow direction have a relative imprecision or incidence of almost $\pm\ 35° \div 60°$, in function of the probe geometry, resulting in a higher yaw/pitch applicable range than Pitot probes, as shown in figure 3.16.

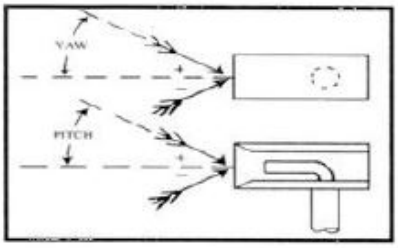

Figure 3.17: Kiel head yaw and pitch angle, [19]

Considering keeping the same probe, results that the probe insensitivity range rises by increasing the external diameter, therefore the inner geometry does not affect the probe performance in terms of yaw and pitch angle insensitivity. [20]

Therefore, a degradation of the external surface could give an error reading pressure from the true pressure.

To obtain a pressure measurement at a specified point in a gas stream, therefore, the pressure is usually sensed by a probe, which is usually a Kiel-head probe due to its great range of insensitivity, and then conveyed to a transducer.

As seen previously, the two reference engines have different transducers types: in the V2500 are installed piezoresistive transducers, silicon capacitive type, while in the CFM56 are installed piezoelectric transducers, quartz capacitive type.

Production aerospace transducers generally report a total error band. Total error band specifications are meant to convey the installed performance when any combination of realistic environmental factors may be present.

Refer to [21], below are shown the characteristics between the piezoresistive

transducer and piezoelectric transducer.

The piezoresistive transducer presents a total error band $\pm \leq 0.1\%FS$ (Full Scale) while the piezoelectric transducer presents a total error band $\pm \leq 1\%FS$.

The main contributing factors to total band error are described below., according with [22]

Total error band is inclusive of the static error band:

$$static\ error\ band = \sqrt{nonlinearity^2 + hysteresis^2 + repeatibility^2} \tag{3.21}$$

- Non-linearity is defined as the maximum deviation of any calibration point on a specified straight line, during any one calibration cycle

- Hysteresis is defined as the maximum difference between output readings, at any pressure value within the specified range, when the value is approached first with increasing and then with decreasing pressure

- Repeatability is defined as the ability of a transducer to reproduce output readings when the same pressure value is applied to it consecutively, under the same conditions, and in the same direction

The overall contribution of hysteresis and repeatability to the static error band is typically less than 10% in silicon capacitive type, due to the nearly perfectly elastic nature of the mono-crystalline silicon pressure sensor combined with the low level of stress applied at full scale. Therefore, Non-linearity is the largest contributing component of the static error band. The static error band of a pressure transducer is typically ±0.1% FS.

A great contribution to the total error band is given from thermal zero shift, which is normally the single largest error source in general purpose pressure transducers together with thermal sensitivity shift.

Thermal sensitivity shift and thermal zero shift define the effects on sensitivity and zero measurement output of operation at operating temperatures other than a normal ambient temperature of 24°C.

The thermal zero drift, which is measured as $\mu V/°C$, causes a constant error that exists over the full range of measurement of the instrument and it can be treated as a bias and periodically tared. Therefore, the thermal zero drift is normally removable by calibration.

Figure 3.18 shows the effect on the output of the thermal zero shift and the thermal sensitivity shift.

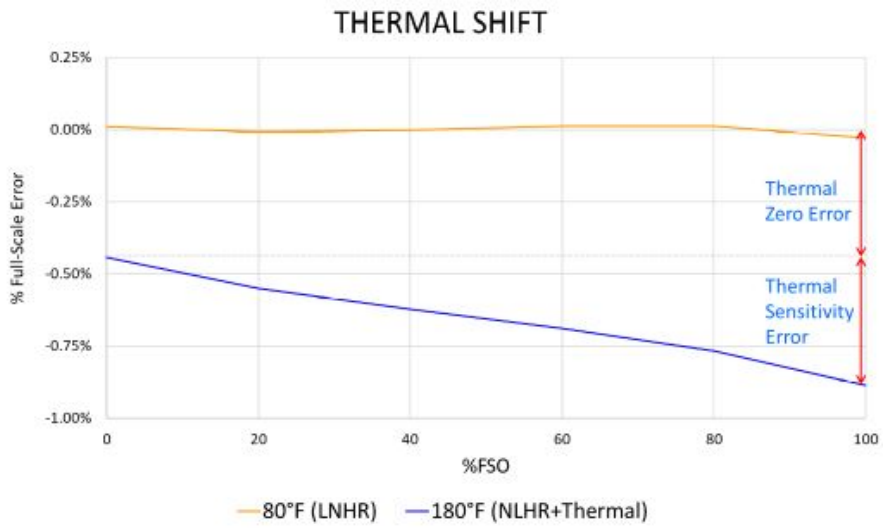

Figure 3.18: Pressure Transducer Thermal Zero and Sensitivity Shift, [22]

In conclusion, the temperature effect on a pressure sensor will be negligible when used at the same laboratory temperature at which it is calibrated. This, however, is not practical for engine measurements.

The pressure transducers can be optimized for different temperature conditions through temperature compensation active or passive.

Regarding the piezoresistive transducer, in passive compensation the span compensation is accomplished by using a series resistor with constant voltage excitation to compensate for the loss of strain sensitivity of silicon piezoresistors with increasing temperature, reaching a deviation of $\pm 0.01\%$ FS/°C, while in the active compensation where the piezoresistive pressure sensors are conditioned by the use of embedded digitally-programmed electronics, temperature sensitivity may be controlled to within $\pm 0.001\%$ FS/°C.

Regarding the piezoelectric transducer is possible with the addition capacitor to give a temperature sensitivity in the range $\pm 0.03 \div 0.2\%$ FS/°C, which is slightly higher than the piezoresistive transducer.

Regarding the drift, both types of transducers show small value: $\leq 0.1\%$FS/year for the piezoresistive transducer, while $\leq 0.5\%$FS/year for the piezoelectric transducer.

The operating temperature capability for both types of transducers is about 540°C, but, as shown in the reference engine, there are regions of a gas turbine, which are hotter, where dynamic gas path pressures are required to be measured.

In these high-temperature environments, the preferred way of measuring the pressure is use of a non-resonant semi-infinite tube SIT system which removes the pressure transducer from the very hot environment by a distance of up to 1 m. [23]

In figure 3.19 a schematic representation of an SIT system is given.

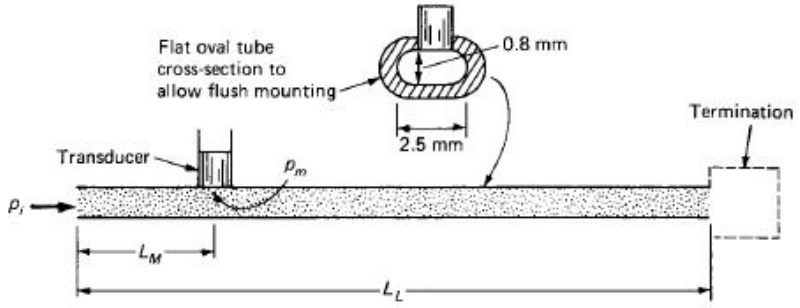

Figure 3.19: Semi-infinte tube, [23]

Where:

- L_M is about 90 cm maximum
- L_M is about 548 cm minimum

The theory behind the SIT design is that for a sufficiently long tube (semi-infinite), pressure fluctuations at the measuring station will have attenuated to small enough values at the far end that their reflection back to the measuring station will be very small, giving negligible measurement errors.

Despite this, in the engines taken as a reference, this technology was not found. A possible explanation for this choice by the manufacturer could be that the length of the pressure line is not consistent, therefore the error given from not using an SIT system is negligible.

3.3.1 Error source: flow characteristics

Regarding the influence of flow characteristics on probe reading the only two effects that can have a significant influence in this instance are compressibility and turbulence in the flow field.[24] [19]

Regarding all Kiel-head probes there is a local speed range in which the critical angle remains constant, this means that the probe in this range is not sensitive to compressibility, as shown in figure 3.20.

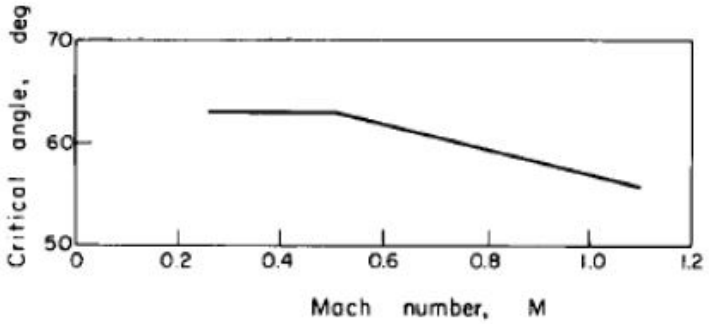

Figure 3.20: Correlation between critical angle and local Mach number for Kiel-head probes, [19]

A steady-calibrated probe in an unsteady and turbulent environment may result in a reading as erratic as lower is the pitch and yaw insensitivity range of the probe itself. This is due to the primary effect of turbulence, which features a time distribution of additional velocity components generated by bi-dimensional vortexes.

As Chue [19] reported, *"For the usual turbulence intensity encountered in pipe and wind-tunnel flow, the turbulence error is small, e.g. for a turbulence intensity of 20%, which is too high for practical situations, the impact pressure reads high by only 2% if the static pressure is assumed to be correctly measured".*

According with [20], the bi-dimensional turbulence intensity level of the flow, which layout is reported in figure 3.21, can be written as:

$$i[\%] = \frac{v}{U} \tag{3.22}$$

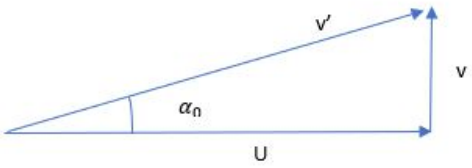

Figure 3.21: A general speed vector composition useful to analytically threat bi-dimensional turbulence

Where:

- U = free-stream flow speed

- v or w = are the turbulent vortexes induced speed components on the plane orthogonal to the probe longitudinal axis
- α_0 = actual angle of attack

Therefore, considering the limit case of α_0 equal to the maximum positive or negative critical angle, it is possible to define the turbulence intensity above which the probe's accuracy decreases:

$$i_{lim} = \tan \alpha_{cr} \tag{3.23}$$

This leads to the conclusion that until the flow turbulence intensity remains under 70%, which is the limit turbulence intensity as calculated through equation 3.23 considering a medium Kiel-head critical angle of 35°, the Kiel-head probe is not sensitive to turbulence induced errors.

A correlation between total pressure read by Kiel-head probe and the turbulence intensity with a CFD evaluation is reported in figure 3.22

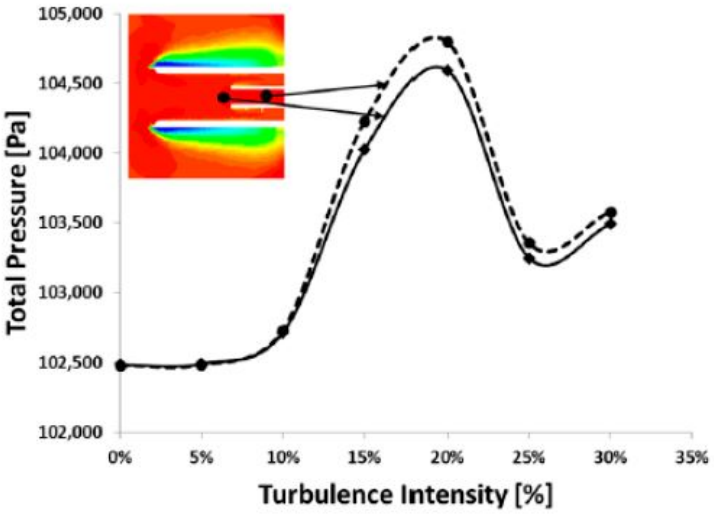

Figure 3.22: Correlation between total pressure read by Kiel-head probe and the turbulence intensity with a CFD evaluation, [24]

The stagnation pressure in figure 3.22 features a peak at 17 % of intensity followed by a steep decrease that is due to a possible separation.

Nevertheless, not considering this peak due to separation,the total pressure felt differs from the free-stream one at almost 10% of turbulence intensity.

This result does not agree with the previously specified limit intensity but, in first time, very different turbulence models have been used because the figure

features a three-dimensional model, and in second time, in the previous study a lot of real aspects, as well as phenomena, have been neglected.

It is critical to understand the relationship between total pressure read by the probe and turbulence because, for example, downstream-the-rotor mounted probes are subjected to important pressure fluctuations owing to wake vortexes generated by the relative motion of rotor blades ahead the probe axis.

In general, fluctuations in turbo-machines can be subdivided into three categories.

- Periodic, which in general, are produced by the rotation of the blades. Other factors that may cause this kind of fluctuations may be the presence of shock waves and the interaction among secondary flow rates, which may include bleed and bypass ones, and the core primary flow
- Nearly periodic, which are caused by large domain unsteady phenomena, such as rotating stall as well as compressor's surge
- Stochastic, which are caused by phenomena such as intermittent blade flutter, boundary layer separation, unsteady transition as well as turbulence

Chapter 4

Test case

In this chapter, for each test case presented, the parameters used to define the error for each type of problem will be briefly summarized before moving on to the construction of the test case in question. A comparison with the literature will also be presented, if available.

Another main objective of this is to choose in which area of the engine to apply the test case, taking into account in which station the error could occur or in which station the error occurs with greater magnitude.

For all test cases presented the station engine identified is the EGT.

- Test case 1 - The temperature and the internal flow Mach number Ma_J have the greatest influence on the error highlighted in this study. Because the mach junction number is independent of the section, the only parameter left to define the section where the test case should be applied is the temperature. The EGT section shows a higher temperature between the sections sensed.

- Test case 2 - Temperature and exposure hours have the greatest influence on the error highlighted in this study. With only three temperature drift curves, it was decided to apply the test case in the region where the temperature was closest to the drift curves, the EGT section is identified like it.

- Test case 3 - Because hot spots can dramatically increase the erosion and sulfidation of metal surfaces, the temperature is the parameter that influenced the error highlighted in this study. and as identified previously, the EGT section has a higher temperature than the other sections.

4.1 Test case 1 - Velocity, conduction and radiation error

The total error in temperature measurement is calculated from three individual errors, namely velocity error, conduction error, and radiation error. As all these errors reduce the measured gas temperature, uncertainty analysis leads to the direct addition of all these errors to the measured value T_J to get the actual gas temperature T_T.

The velocity error can be increased, or reduced, by changing the internal flow Mach number Ma_J , regulating the inlet-to-exit area ratio of the probe.

The conduction error can be increased, or reduced, by a variation of the convective heat transfer coefficient h_C, which is directly coupled to flow velocity inside the sensor.

The radiation error can be increased, or reduced, by a variation of the convective heat transfer coefficient h_C, like the conduction error.

As a result, the main factor is the Mach number of the flow within the sensor tube that depends on the flow area ratio of the tube inlet AE and the bleed holes AB (see figure 3.9).

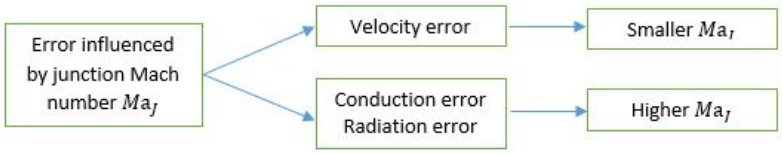

Figure 4.1: Best Ma_J to reduce the velocity, conduction and radiation error

As shown in figure 4.1, Kiel's internal Mach number Ma_J is a trade-off between velocity error on one side and conduction and radiation error on the other side: to get an optimum result the internal Mach number should be small enough to keep the velocity error small, but high enough to avoid large conduction and radiation errors.

During the probe design phase, a minimized recovery error in realistic cases can be realized with internal Mach numbers between 0.05 and 0.15 but in applications with very high radiation and conduction errors (high temperatures) the internal Mach number, which is the most important factor should be chosen in a range of around 0.15.

Another parameter to be considered in the design is the L/D ratio that influences the conduction error: in practical probe design, L/D = 10÷15 seems to be achievable and sufficient regarding the mechanical stability of the junction for wires normal to flow.

4.1.1 On-design

Before proceeding with the development of the test case, it is necessary to define the installation of the thermocouple in the reference engine CFM56, which is chosen between the two reference engine to simulate the test case.

The EGT, which presents a value equal to 1188 K, is not measured in the main stream of the LPT air, it is measured by a thermocouple located in the interior of the vane as shown in figure 4.2.

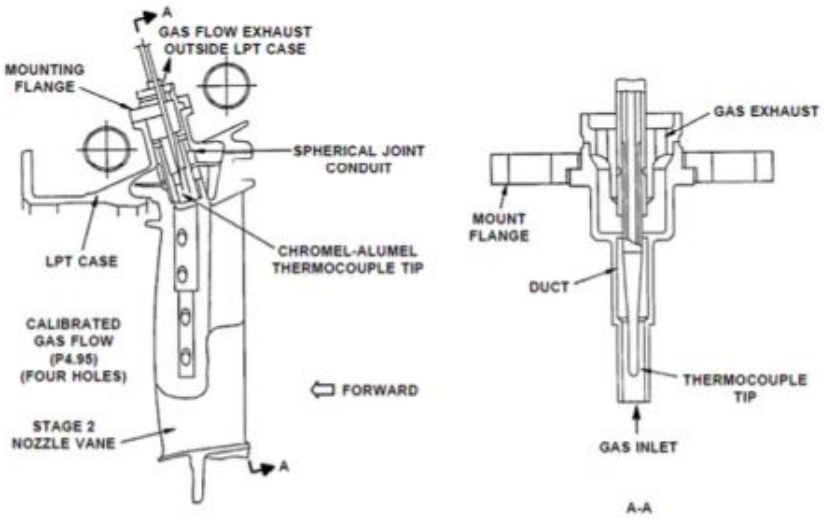

Figure 4.2: Schematic of the EGT sensor - CFM56, [4]

Considering that the real local Mach number in the application is not exactly known and that for the reference engine CFM56 the EGT is in the 2nd stage of LP turbine, therefore, a free-stream Mach number is assumed to be 0.8 like a possible turbine's Mach design.

To obtain an accurate measurement of the conduction and radiation errors, a heat transfer analysis of the probe would be required to obtain the mount temperature T_M and the wall temperature T_W.

Following it will present a method to obtain valid values in first approximation, without to recur necessarily to heat transfer analysis.

The following analyses will be conducted using 3.2 mm wire diameter thermocouple, being the same diameter used to characterize the drift for bare wire KP and KN thermoelements in low-oxygen content atmosphere, shown in figure 3.14

Moreover, taking into account that the EGT work under the effect of a gas combustion, specific heat gas combustion $c_p^{'}$ is taken equal to $1184\frac{J}{Kg\ K}$, the R*(constant gas/molar mass) is taken equal to $293.77\frac{J}{Kg\ K}$, and the $\gamma^{'}$ is taken equal to 1.33.

Velocity error

Taking into account the considerations made previously, to obtain a Mach number junction Ma_J, in accordance with the range that has been highlighted previously, a ratio AE/AB equal to 4 is defined.

This ratio, referring to equation 3.10, return a Mach number junction Ma_J equal to 0.137.

As shown in 4.2, the flow it will be considered parallel to the wire. Under these conditions the recovery factor recommended for bare thermocouple should be in the range R = 0.86 ± 0.09, but not having characterized the probe, in first approximation, is assumed the rake shaft like a cylindrical body under cross-flow conditions, which the recovery factor value is given to 0.68. [14]

Referring to the equation 3.9, a velocity error results equal to 1.18 K.

Conduction error

Taking into account the considerations made previously, the ratio L/D equal to 10 is defined.

Considering a wire diameter equal to 3.2 mm, is obtained a length of thermocouple exposed equal to 320 mm.

From Sutherland's formulas 4.1, a dynamic viscosity equal to 4.60 $10^{-5} \frac{Kg}{m\ s}$ is obtained for the temperature of 1188 K.

$$\mu = S\frac{T^{3/2}}{\chi + T} \tag{4.1}$$

Where:

- $S = 1.4610^{-6}\ \frac{Kg}{m\ s\ K^{1/2}}$
- $\chi = 110K$

An approximation of the velocity inside the probe is given from equation 4.2 and 4.3: considering the Mach number junction Ma_J, which is defined as equal to 0.137, and the total temperature, which is defined as equal to 1188 K, a velocity inside the probe is equal to 93 m/s.

$$T = \frac{T_0}{1 + \frac{\gamma' - 1}{2} Ma_J^2} \tag{4.2}$$

$$V = Ma_J\ \sqrt{\gamma'\ R^*\ T} \tag{4.3}$$

Having defined the velocity inside the probe and the dynamic viscosity, it is possible to define Reynolds number, and consequently, the Nusselt number and the convective heat transfer coefficient h_C, which results equal to 411 $\frac{W}{m^2 K}$.

Regarding the mounting temperature, it is assumed that with a bleed from the first stages of the HPC, which have the same pressure to be able to thus the cooling, it is possible to maintain the mounting temperature at 150 k less than the total temperature inside the probe.

The thermal conductivity of thermocouple material k_S is 100 $\frac{W}{m\ K}$ while for the gas, considering the pressure and the temperature in operation condition, a value of the thermal conductivity is given equal to 0.09 $\frac{W}{m\ K}$.

Referring to the equation 3.14 is obtained a conduction error equal to 2.09 K.

Radiation error

Referring to the equation 4.5, it is necessary to estimate the surface wall and the surface thermocouple exposed: the surface wall is estimated 1700 mm^2 considering an internal diameter equal to about 5.2 times the diameter of wires for MIMS configuration [7], while the surface thermocouple exposed is estimated 643 mm^2.

The rake shaft temperature rises from a low value, at the cooled engine casing, to a stable value between the static and total temperatures, which is determined by the shaft's recovery factor and the radiation heat exchange with surrounding surfaces, which will be neglected in first approximation.

This analysis allows to arrive at an approximation of the rake's temperature equal to 1151 K, following the equation 4.4, where free-stream static temperature T_S is defined through the isentropic equation and equal to 1074.5 K.

$$T_W = T_S \left(1 + R\frac{\gamma' - 1}{2} Ma_F^2\right) \tag{4.4}$$

Referring to the equation 4.5, a radiation error equal to 2.94°C is obtained.

Considerations

Figure 4.3 shows the influence of the different effects on the measurement of total temperature. A deviation from the total temperature of 0.53% is detected.

The deviation is mainly caused by the radiation which results 0.25% in according with the figure 3.11.

A correction with the calibrated recovery factor only eliminates the velocity and the conduction error. Therefore an error of 0.25% will remain after the correction. This is in the same order as the thermocouple error and must not be neglected.

The comparison between the results of this investigation and data from the literature shows an overall deviation of this work in good approximation valid. The overall deviation from the total temperature in [14] is equal to 0.9%. The low difference can be related to the different temperatures and to the different free-stream Mach numbers, on which the influence of separate effects is studied. Strongly

deviation is detected for the radiation error being this work evaluated about 200 K less, while the velocity and the conduction error give the same percentage of deviation.

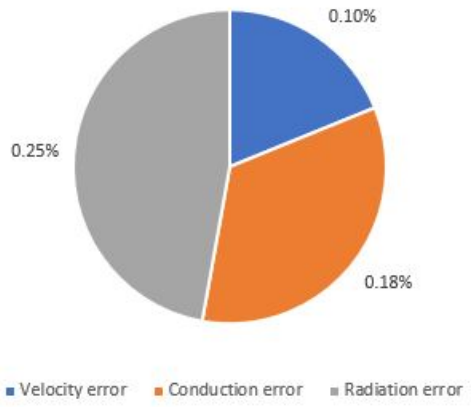

Figure 4.3: Deviation of a typical total temperature measurement and influence of separate effects

The other errors like the thermocouple error still have to be added. The table 4.1 shows the single parts identified in the chain of the thermocouple with the relative inaccuracy. The ΔT obtained in the analysis is related to the temperature of the EGT in °C.

Kiel's probe	6.21 °C	0.68%
Type K thermocouple	3.66°C	0.4%
TC extension wire	0.91°C	0.1%
Reference junction	2.28°C	0.25%
DAQ System	-	«1 - neglected
tot.	13.06°C	1.43%

Table 4.1: Thermocouple chain Inaccuracy

Overall, is detected an inaccuracy from the real total temperature equal to 13.06 °C, which corresponding in percentage to 1.42% respect 915°C EGT temperature.

4.1.2 Off-design

Considering a geometry change of the Kiel's probe inlet AE and the bleed holes AB, due to erosion or thermal dilatation, in figure 4.4 is presented the percentage variation of the velocity, conduction, and radiation error.

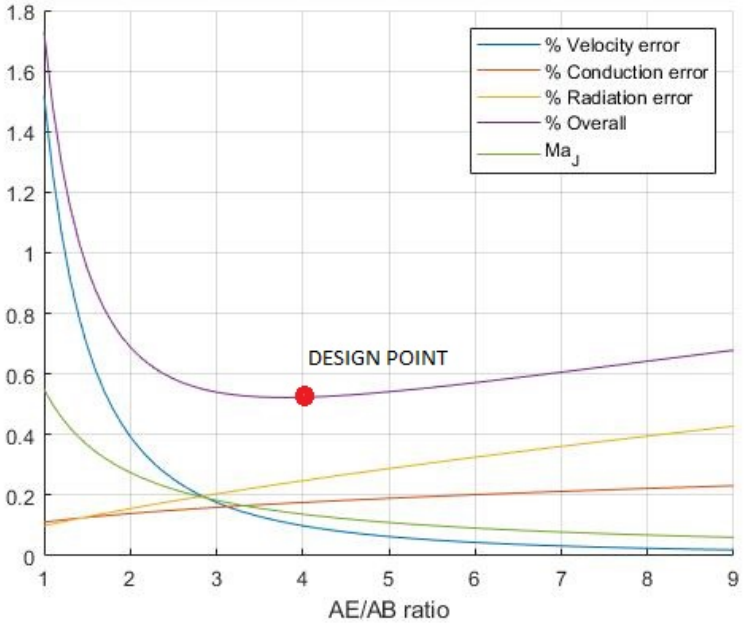

Figure 4.4: Effect of AE/AB ratio on velocity, conduction and radiation error to 1188 K

The change of AE/AB ratio is followed by a change of the Mach number junction Ma_J, that as shown in the figure 4.1, is followed by a redefinition of inaccuracy percentage due to the velocity, conduction, and radiation error.

As shown in figure 4.4, considering the absurd situation in which AE /AB changes its value to +50 % from the design point, an overall $\Delta\%overall$ equal to 0.04% occurs regarding the design configuration, returning a Kiel's probe inaccuracy equal to 6.77 K, while for -50 % from the design condition, an overall $\Delta\%overall$ equal to 0.15% regarding the design configuration, returning a Kiel's probe inaccuracy equal to 8.07 K.

This low variation from design conditions is justified because the most predominant error in high-temperature measurement is radiation error, which increases exponentially above 1300 K, while the velocity and the conduction error are strongly influenced by the Mach number junction Ma_J, which have no significant values, going only outside the ideal range and, at the same time, outside the range in which the speed error increases consistently.

4.2 Test case 2 - Aging/Drift and Inhomogeneities of the thermocouple

The only thermocouple part subjected to oxidation in the MIMS with exposed bare wire junctions configuration is the junction, which is the only part of the thermocouple exposed to the surrounding environment. But nevertheless, changes at the thermocouple junction usually have no effect on drift because the junction is assumed to be at constant temperature. As a result, only the change caused by the short-range order effect contributes to drift in the MIMS configuration with exposed bare wire junctions. For the same reason, the interaction with the sheath does not contribute to thermocouple drift.

Referring at the figure 3.14, after 400h for exposition at 1000°C, results a drift equal to +100 μV for the KP thermoelement, while a drift equal to +15 μV for the KN thermoelement.

Overall the short-range order effect produces a positive contribution to drift of 115 μV after 400 h.

From the NIST online database [25] has been obtained the type K Thermocouples Coefficients, shown in table 4.2.

c_0	-0.17600413686 10^{-1}	c_7	-0.320207200030 10^{-18}
c_1	0.389212049750 10^{-1}	c_8	0.971511471520 10^{-22}
c_2	0.185587700320 10^{-4}	c_9	-0.121047212750 10^{-25}
c_3	-0.994575928740 10^{-7}	a_0	0.118597600000 10^{0}
c_4	0.318409457190 10^{-9}	a_1	-0.118343200000 10^{-3}
c_5	-0.560728448890 10^{-12}	a_2	0.126968600000 10^{3}
c_6	0.560750590590 10^{-15}	-	-

Table 4.2: Type K Thermocouples Coefficients

The emf-Temperature relationship is obtained with the following equation and shown in the figure 4.5:

$$emf = \sum_{i=0}^{n} c_i \left(t_{90}^i\right) + a_0 \, e^{a_1 (t_{90} - a_2)^2} \; i = 0, ..., n \tag{4.5}$$

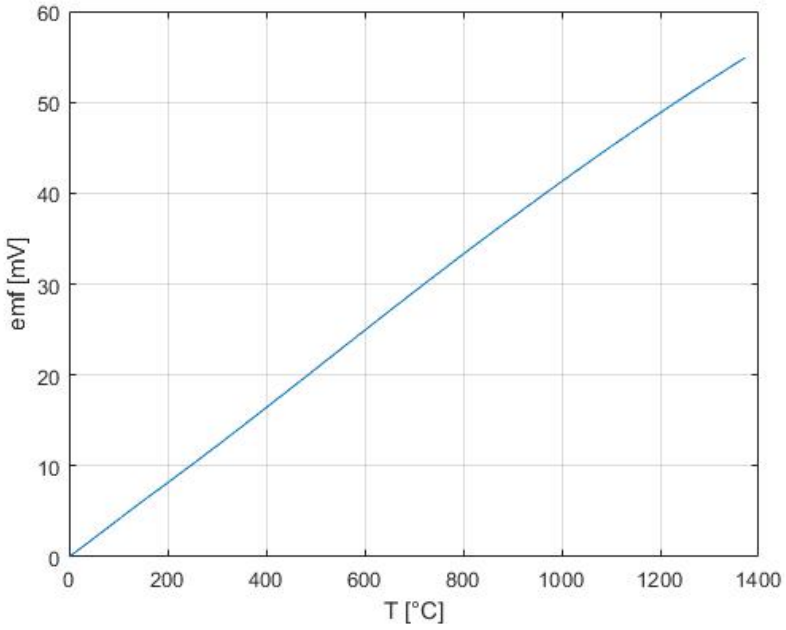

Figure 4.5: emf - Temperature relationship for type K thermocouple

At the temperature of 915°C results a thermocouple output equal to 37.9249 μV: considering that the same type k thermocouple has a contribution to drift of +115 μV after 400 h, the overall output result to be equal to 38.0399 μV , which corresponds to ΔT equal to 2.5°C.

The contribution of the drift for a thermocouple in configuration MIMS with exposed junction, with wire diameter 3.20 mm after 400 h to 1000°C results to be 0.27%.

Adding these results to the overall error by velocity, conduction, and radiation error, a value prediction equal to 15.56°C is obtained, which corresponds to 1.70% with respect to 915°C EGT temperature.

4.3 Test case 3 - Lost of one thermocouple

Assuming the loss of a thermocouple due to the missing probe tip or open sensor circuits, as discussed previously, the average value will be calculated from the weighted average of the valid sectors because an error message *Signal disagree'* is generated by the EEC due the sector that has 200°C discrepancies compared to the average of the other sectors.

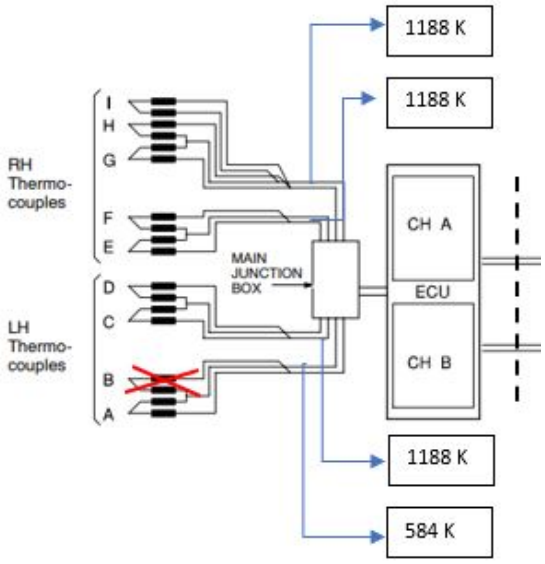

Figure 4.6: Lost of one thermocouple

In the case in which the sector is not excluded, for example, because the logic has not been implemented, is obtained an untrue temperature read compared to the real total temperature equal to 1037 K, according to the the following equation:

$$EGT_{read} = \sum_{j=1}^{N} \frac{\sum_{i=1}^{n} T_i}{n_j} \; i = 1, ..., n \; j = 1, ..., N \tag{4.6}$$

Where:

- n = number of thermocouples in each sector
- N = number of sector

Conclusions

This chapter represents the end of the study carried out, by the undersigned, at the ILA (Institut für Luftfahrtantriebe) sited in the University of Stuttgart.

Within the proposed work, the author tried to analyze the contributions of each component in the chain of temperature and pressure measurement systems, to the inaccuracy of the two systems.

In addition, it has been conducted a forecast campaign about three test cases developed, according to the errors highlighted in the two chain systems.

In other words, the present study dealt with the comprehension of how much and in which way the instrumentation, in terms of temperature and pressure measurements, used in today's engine can affect the precision of the real temperature and pressure inside the gas turbine engine

In this way, the aim of this study consisted in performing, firstly, a deeper understanding of the contributions of different parameters involved in defining the system's inaccuracy and, secondly, the formulation of inaccuracy forecast for the errors highlighted during this work.

Another feature on which the attention has been focused was been to get an idea of how modern engine identifies and insulates sensor faults. This analysis led to the conclusion that due to all the potential engine failures, isolating sensor faults is not always easy, because some inputs take into account other parameters in the calculation phase. Therefore, the manufacturers don't give specific instructions on the fault strategy. The only conclusion that can be highlighted is how the fault strategy heavily depends on the engine's control and monitoring logic.

During the first part of these six months, detailed bibliography research has been conducted in order to gather sufficient data to focus the study but, owing to the very broad and variegated field such as this one debated, the link at single details for each component of the chain it turned out to be necessary.

For the temperature measurement system, despite the results are not highly representative of the real physics of the studied phenomena as some strong approximations, the same results constitute a valid tool to state that:

- at temperature close to 1000°C the radiation error is the main cause of the temperature deviation, together with thermocouple accuracy and the error

identified for the reference junction. Considering the absurd situation of a change of ±50% from the design point AE/AB ratio, the plus deviation respect to the intrinsic one is irrelevant.

- in MIMS configuration with exposed junction, the short-range order is the main drift contribution, because the junction part exposed to flow can be assumed that is at a constant temperature, so it does not play any role in drift. With a diameter of 3.2 mm, the deviation is forecast to be equal to 0.27%, which being in the same order as the thermocouple type K error must not be neglected.
- the lost of one thermocouple due to missing probe tip or open sensor circuits leads the internal logic to exclude the sector because the discrepancy compared to the average of the other sectors is above the limit.

For the pressure measurement system, the largest source of the error is given from the probe, identified in Kiel's probe design as it has large ranges of yaw and pitch insensitivity. The influence of flow characteristics on probe reading could lead to deviations from the real pressure. Regarding the sensitivity to compressibility, for Mach number upper 0.5 a critical angle decreases while for the effect of the turbulence, keeping in mind that in turbo-machinery turbulence intensities won't overwhelm a 10% value, the errors will be negligible every time. Being that the Kiel's head yaw and pitch insensitivity depend on the external diameter, degradation due to erosion of the external surface of the shroud could be the cause of a deviation from real pressure.

Appendix A

MATLAB script

A.1 Dipendence of the Ma_J to AE/AB ratio

```
gamma=1.409
Ma_F=0:0.1:1;
ratio=linspace(1,10,200)
for i=1:length(Ma_F)

%Ma_j to AE/AB ratio
Maj=Ma_F(i)./ratio.*(1+(gamma-1)/2*Ma_F(i)).^(-1/(gamma-1));
end

%recovery factor: reccomends for wire thermocouple normal to flow
R=0.9
Tt=linspace(288,1490,10);
for i=1:length(Tt)

% Veloity error - [K]
Ve=(1-R)*(((gamma-1)/2*Maj.^2)./(1+(gamma-1)/2*Maj.^2)).*Tt(i)
```

A.2 Effect of the L/D ratio on conduction error

```
kg=0.12;                                %[W/(m*K)]
ratio=[ 5, 10, 15, 20]
D=0.005                                 %[m]
L=D*ratio                               %[m]

%Reynold number --> Re
Re=200:100:6000

%Valutiamo il numeor di Nusselt --> Nu
Nu=(0.44+0.06)*Re.^(1/2);

%Valutiamo heat transfer coefficient --> h_c
hc=Nu.*kg./D;
ks=100 ;                                %[W/(m*K)]
for i=1:length(ratio)
    for j=1:length(Re)

%Conduction error normalizzato
Ce_norm(i,j)=1/(cosh (L(i)*(4*hc(j)/(D*ks))^(1/2)))
    end
end
```

A.3 Velocity, conduction and radiation error on-design

```
ratio_1=4;                              %DESIGN

%Valutiamo gas combusti
gamma=1.409;
cp_primo=1184;                          %[J/(kg K)]
R_primo=293.77;                         %[J/(kg K)]
gamma_primo=(cp_primo/R_primo)/(cp_primo/R_primo-1);

%recovery factor: reccomends for wire thermocouple parallel to flow
R=0.68   ;
Ma_F=0.8   ;                            %Supposed like Ma_D LPT
Tt=915+273;                             %[K]
Maj=Ma_F/ratio_1.*(1+(gamma_primo-1)/2*Ma_F)^(-1/(gamma_primo-1));

%Velocity error
Ve=(1-R)*(((gamma_primo-1)/2*Maj^2)./(1+(gamma_primo-1)/2*Maj.^2))*Tt

kg=0.09;                                %[W/(m*K)]
ratio=10
D=0.0032                                %[m]
L=D*ratio                               %[m]
chi=110;                                %[K]

S=1.46*10^-6;                           %[kg/(m*s*K^1/2)]

%Sutherland law -->dinamic viscosity
mu=S*Tt^(3/2)/(chi+Tt) ;                %[kg/(m*s)]

Ts=Tt/(1+(gamma_primo-1)/2*Maj^2)
cost=292.43

%Velocity inside the probe
V=Maj*(gamma_primo*cost*Ts)^0.5   %[m/s]

rho=0.32;                               %[Kg/m^3] -->rho=P/(Ra*T)

%Reynold numeber --> Re
Re=rho*V*D/mu

%Nusselt number --> Nu
%Nu=(0.44)*Re^(1/2)                     %wires normal to flow
Nu=0.085*Re^(0.674)                     %wires parallel to flow

```

```
%Heat transfer coefficient
hc=Nu*kg/D;
ks=100  ;                                   %[W/(m*K)]

%Conduction error
Ce_norm=1/(cosh (L)*(4*hc/(D*ks))^(1/2))
diffT=150                                   %[K]
Ce=diffT*Ce_norm                            %[K]

eps=0.2;
sigma=5.67*10^-8;
Ts_w=Tt/(1+(gamma_primo-1)/2*Ma_F^2)
Tw=Ts_w*(1+ R* (gamma_primo-1)/2*Ma_F^2)

%Surface thermocouple
ATC=2*pi*D/2*L*2                            %[m^2]

%Surface wall
AW=2*pi*(D/0.19)/2*(L)                      %[m^2]

%Radiation error
Rer=sigma*eps/hc*(Tt^4-Tw^4)*1/(1+ATC/AW+(1-eps))

%Percentage error
err_per_V=Ve/Tt*100
err_per_Ce=Ce/Tt*100
err_per_Rer=Rer/Tt*100
tot=Ve+Ce+Rer
```

A.4 Effect of AE/AB ratio on velocity, conduction and radiation error

```
ratio_1=1:0.1:9;

%Valutiamo gas combusti
gamma=1.409;
cp_primo=1184;                          %[J/(kgK)]
R_primo=293.77;                         %[J/(kgK)]
gamma_primo=(cp_primo/R_primo)/(cp_primo/R_primo-1);

%Recovery factor: recommends for wire thermocouple parallel to flow
R=0.68   ;
Ma_F=0.8   ;                            %Supposed like Ma_D LPT
Tt=915+273;                             %[K]
Maj=Ma_F./ratio_1.*(1+(gamma_primo-1)/2*Ma_F)^(-1/(gamma_primo-1));

%Velocity error
Ve=(1-R).*(((gamma_primo-1)./2*Maj.^2)./(1+(gamma_primo-1)/2*Maj.^2))
    *Tt

kg=0.09;                                %[W/(m*K)]
ratio=10
D=0.0032                                %[m]
L=D*ratio                               %[m]
chi=110;                                %[K]
S=1.46*10^-6;                           %k[g/(m*s*K^1/2)]

%>Sutherland law --> dinamic viscosity
mu=S*Tt^(3/2)/(chi+Tt) ;                %[kg/(m*s)]

Ts=Tt./(1+(gamma_primo-1)./2*Maj.^2)
cost=292.43

%Velocity inside the probe
V=Maj.*(gamma_primo*cost*Ts).^0.5    %[m/s]

rho=0.32;                               %K[g/m^3] -->rho=P/(Ra*T)

%Reynolds number --> Re
Re=rho*V.*D./mu

%Nusselt number --> Nu
%Nu=(0.44)*Re.^(1/2);                   %Wires normal to flow
Nu=0.085*Re.^(0.674)                    %Wires parallel to flow

```

```
%Heat transfr coefficient
hc=Nu.*kg/D;
ks=100  ;                                   %[W/(m*K)]

%Conduction error
Ce_norm=1./(cosh (L).*(4*hc./(D*ks)).^(1/2))
diffT=150                                   %[K]
Ce=diffT*Ce_norm


eps=0.2;                sigma=5.67*10^-8;
Ts_w=Tt/(1+(gamma_primo-1)/2*Ma_F^2)
Tw=Ts_w*(1+ R* (gamma_primo-1)/2*Ma_F^2)

%Surface thermocouple
ATC=2*pi*D/2*L*2                            %[m^2]

%Surface wall
AW=2*pi*(D/0.19)/2*(L)                      %[m^2]

%radiation error
Rer=sigma*eps./hc.*(Tt^4-Tw^4)*1/(1+ATC/AW+(1-eps))

%Percentage error
err_per_V=Ve./Tt*100
err_per_Ce=Ce./Tt*100
err_per_Rer=Rer./Tt*100
tot=Ve+Ce+Rer
tot_perc=tot/Tt*100
```

A.5 emf - Temperature relationship for type K thermocouple

```
%Type K coefficients
c0=-0.176004136860*10^(-1)
c1=0.389212049750*10^(-1)
c2=0.185587700320*10^(-4)
c3=-0.994575928740*10^(-7)
c4=0.318409457190*10^(-9)
c5=-0.560728448890*10^(-12)
c6=0.560750590590*10^(-15)
c7=-0.320207200030*10^(-18)
c8=0.971511471520*10^(-22)
c9=-0.121047212750*10^(-25)
a0=0.118597600000*10^0
a1=-0.118343200000*10^(-3)
a2=0.126968600000*10^(3)
x=0:0.5:1372
for i=1:length(x)
y(i)=c0+c1*x(i)+c2*x(i)^2+c3*x(i)^3+c4*x(i)^4+c5*x(i)^5+c6*x(i)^6+c7*
    x(i)^7+c8*x(i)^8+c9*x(i)^9+a0*exp(a1*(x(i)-a2)^2)
end

%emf to 1188 K
t1=915
y0=c0+c1*t1+c2*t1^2+c3*t1^3+c4*t1^4+c5*t1^5+c6*t1^6+c7*t1^7+c8*t1^8+
    c9*t1^9+a0*exp(a1*(t1-a2)^2)
y1=37.9249+115*10^(-3)
```

Bibliography

[1] Alexander Von Moll, Dr. Alireza R. Behbahani, Gustave C. Fralick, John D. Wrbanek, and Dr. Gary W. Hunter. «A Review of Exhaust Gas Temperature Sensing Techniques for Modern Turbine Engine Controls». In: *Integrated Distributed Engine Controls*. Cleveland, Ohio, July 2014 (cit. on p. 2).

[2] *V2500 A1 A5/D5 Familiarization*. MTU Maintenance (cit. on pp. 5, 7, 8).

[3] *I.A.E V2500 course notes* (cit. on pp. 5, 8, 11).

[4] *ATA 71-80 engine CFM56-5A*. Lufthansa technical training. 1999 (cit. on pp. 6–8, 10, 54).

[5] *Training manual - Engine systems, CFM56-5A*. CFMI. 2000 (cit. on pp. 6, 8, 12).

[6] *Training manual - Fault detection and annunciation, CFM56-5A*. CFMI. 2003 (cit. on pp. 14–19).

[7] Helen M. Hoersch, ed. *Manual of the use of the thermocouples in temperature measurements*. ASTM editor, 1993 (cit. on pp. 23–30, 38, 56).

[8] M. Scervini. *Thermoelectric materials for thermocouples*. URL: `https://www.msm.cam.ac.uk/utc/thermocouple/pages/MicheleScerviniMainPage.html` (cit. on pp. 23, 27, 39, 40).

[9] E. S. Webster. «Drift in Type K Bare-Wire Thermocouples from Different Manufacturers». In: *TEMPMEKO*. 2016, p. 70 (cit. on p. 25).

[10] M. Scervini and C. Rae. «The Contributions to Drift of Positive and Negative Thermoelements in Type K Bare-Wire Thermocouples». In: *Temperature: Its Measurements and Control in Science and Industry*. Vol. 8. 2013, pp. 564–569 (cit. on pp. 25, 28, 38, 41).

[11] *Recommended Practices for Measurement of Gas Path Pressures and Temperatures for Performance Assessment of Aircraft Turbine Engines and Components*. Advisory Report 245. Advisory Group for Aerospace Research and Development - AGARD, 1990 (cit. on pp. 27, 31).

[12] M. Scervini and C. Rae. «The Contributions to Drift of Positive and Negative Thermoelements in Type K MIMS Thermocouples». In: *Temperature: Its Measurements and Control in Science and Industry*. Vol. 8. 2013, pp. 570–575 (cit. on pp. 28, 38, 40).

[13] *Thermocouple theory and practice*. Tech. rep. labfacility - Temperature process technology (cit. on p. 29).

[14] A. Zeisberger. *Total temperature probes for turbine and combustor applications*. American Institute of Aeronautics and Astronautics. 2007 (cit. on pp. 31, 36, 55, 56).

[15] Steven Tyler Englerth. «An Experimental Conduction Error Calibration Procedure for Cooled Total Temperature Probes». MA thesis. Blacksburg, Virginia: Virginia Polytechnic Institute, 2015 (cit. on p. 31).

[16] D. L. Fish. «Thermocouples and TIT». In: *Service news* 9 (1982), pp. 147–223 (cit. on p. 41).

[17] I.N.Niranjan Kumar V.Naga Bhushana Rao and*, K.Bala Prasad, N.Madhulata, and Naresh Gurajarapu. «Failure mechanisms in turbine blades of a gas turbine Engine –an overview». In: *International Journal of Engineering Research and Development* 10 (2014), pp. 48–57 (cit. on p. 42).

[18] *Operation and Maintenance Manual - revision 7*. Rolls–Royce Corporation. 2003 (cit. on p. 42).

[19] S. H. Chue. «Pressure probes for fluid measurement». In: *Progress in Aerospace Sciences* 16 (1975), pp. 147–223 (cit. on pp. 44, 45, 48, 49).

[20] Gerardo Russo. «Experimental analysis of pneumatic probes in an unsteady environment». MA thesis. Turin: Politecnico di Torino, 2018 (cit. on pp. 45, 49).

[21] Steve Carter, Alex Ned, John Chivers, and Andy Bemis. *Selecting Piezoresistive vs. Piezoelectric Pressure Transducers*. Tech. rep. AN-102. NJ: Kulite Semiconductor Products, Inc, 2018 (cit. on p. 45).

[22] Steve Carter. *Understanding the Pressure Transducer Datasheet: Total Error Band vs. Accuracy*. Tech. rep. TD 1012. NJ: Kulite Semiconductor Products, Inc, 2020 (cit. on pp. 46, 47).

[23] *Application Information*. Tech. rep. Kulite Semiconductor Products, Inc, 2018 (cit. on pp. 47, 48).

[24] S. Bauinger, A. Marn, E. Göttlich, and F. Heitmeir. «Influence of Pressure Fluctuations on the Mean Value of Different Pneumatic Probes». In: *International journal of Turbomachinery Propulsion and Power* (2017) (cit. on pp. 48, 50).

[25] NIST. *Tables of Thermoelectric Voltages and Coefficients - ITS90*. URL: `https://srdata.nist.gov/its90/type_k/kcoefficients.html` (cit. on p. 59).